ICE, CLOUD, and Land Elevation Satellite (ICESat-2) Project

Algorithm Theoretical Basis Document (ATBD) for ATL03g ICESat-2 Receive Photon Geolocation

Prepared By:

Scott B. Luthcke
(NASA/GSFC, Code: 61A)

Teresa Pennington
(SGT/GSFC, Code 61A)

Tim Rebold
(EST/GSFC, Code 61A)

Taylor Thomas
(EST/GSFC, Code 61A)

Goddard Space Flight Center
Greenbelt, Maryland

Foreword

This document is an Ice, Cloud, and Land Elevation (ICESat-2) Project Science Office controlled document. Changes to this document require prior approval of the Science Development Team ATBD Lead or designee. Proposed changes shall be submitted in the ICESat-II Management Information System (MIS) via a Signature Controlled Request (SCoRe), along with supportive material justifying the proposed change.

In this document, a requirement is identified by "shall," a good practice by "should," permission by "may" or "can," expectation by "will," and descriptive material by "is."

Questions or comments concerning this document should be addressed to:

ICESat-2 Project Science Office
Mail Stop 615
Goddard Space Flight Center
Greenbelt, Maryland 20771

Preface

This document is the Algorithm Theoretical Basis Document for the ICESat-2 Received Photon Geolocation. The SIPS supports the ATLAS (Advance Topographic Laser Altimeter System) instrument on the ICESat-2 Spacecraft and encompasses the ATLAS Science Algorithm Software (ASAS) and the Scheduling and Data Management System (SDMS). The science algorithm software will produce Level 0 through Level 4 standard data products as well as the associated product quality assessments and metadata information.

The ICESat-2 Science Development Team, in support of the ICESat-2 Project Science Office (PSO), assumes responsibility for this document and updates it, as required, as algorithms are refined or to meet the needs of the ICESat-2 SIPS. Reviews of this document are performed when appropriate and as needed updates to this document are made. Changes to this document will be made by complete revision.

Changes to this document require prior approval of the Change Authority listed on the signature page. Proposed changes shall be submitted to the ICESat-2 PSO, along with supportive material justifying the proposed change.

Questions or comments concerning this document should be addressed to:

Thorsten Markus, ICESat-2 Project Scientist
Mail Stop 615
Goddard Space Flight Center
Greenbelt, Maryland 20771

Review/Approval Page

Prepared by:

Scott Luthcke POD/PPD, Calibration and Geolocation Lead NASA/GSFC Code: 61A Greenbelt, MD 20771	Tim Rebold POD/PPD, Calibration and Geolocation Aerospace Engineer Emergent Inc. @ NASA GSFC
Teresa Pennington POD/PPD, Calibration and Geolocation Systems Engineer SGT Inc. @ NASA GSFC 7701 Greenbelt Rd, Greenbelt, MD 20770	Taylor Thomas POD/PPD, Calibration and Geolocation Aerospace Engineer Emergent Inc. @ NASA GSFC

***** Signatures are available on-line at:** https:// /icesatiimis.gsfc.nasa.gov ***

Change History Log

Revision Level	Description of Change	SCoRe No.	Date Approved

List of TBDs/TBRs

Item No.	Location	Summary	Ind./Org.	Completion Date

Table of Contents

List of Figures

List of Tables

1.0 INTRODUCTION

1.1 Document Overview and Objective

This document is designed to provide both: (1) a general theoretical overview of the algorithms, processing steps and procedures required to provide the Geolocated heights for each ATLAS photon event, and (2) a detailed geolocation algorithm implementation and processing flow specifically designed for the ICESat-2 mission. Algorithm description for the direct and crossover altimeter measurement models, and residual analysis for geolocation parameter estimation (calibration and validation), is provided in the Precision Orbit Determination (*POD), Orbit Design and Geolocation Parameter Calibration ATBD*.

The geolocation of an ATLAS photon event is computed as a function of three complex measurements: (1) the position of the space based ranging instrument from the Precision Orbit Determination (POD) (2) the pointing of the laser pulse from the Precision Pointing Determination (PPD), and (3) the photon event round trip travel time observation measured by the ATLAS instrument. To transform these measurements into geolocated bounce points for each photon event, a variety of models, algorithms, and corrections need to be adopted and applied. These include the determination of the spacecraft (S/C) position and laser pointing within a consistent geodetic reference frame, the correction for atmospheric refraction path delay, ranging and time-tag corrections, the removal of unwanted geophysical effects such as tides, the invariant geoid and rotational deformation.

This topic is arranged in the following manner:

- **Section 2** presents the rigorous geolocation algorithm where the laser pointing, S/C attitude, S/C position, and instrument range and timing biases are known and combined along with the observed photon event round-trip range to produce a geolocated bounce point. The algorithm rigorously includes the light time solution in order to properly compute the transmit and receive leg ranges.
- **Section 3** presents the implementation details of the geolocation algorithms for the ICESat-2 mission including simplifying and resource conserving approximations, as well as data flow and connection to mission data files and products.

1.2 Related Documentation

This section provides the references for this interface control document. Document references include parent documents, applicable documents, and information documents.

1.6.1 Parent Documents

Parent documents are those external, higher-level documents that contribute information to the scope and content of this document. The following ICESat-2 documents are parent to this document.

a) Ground System Requirements Document ICESat-2-GSPM-REQ-0330 ICESat-2
b) Algorithm Theoretical Basis Document (ATBD) for Global Geolocated Photons

1.6.2 Applicable Documents

Applicable documents include reference documents that are not parent documents. This category includes reference documents that have direct applicability to, or contain policies binding upon, or information directing or dictating the content of this document. The following ICESat-2, EOS Project, NASA, or other Agency documents are cited as applicable to this interface control document.

a) Algorithm Theoretical Basis Document (ATBD) for Precise Orbit Determination (POD), Orbit Design and Geolocation Parameter Calibration
b) Algorithm Theoretical Basis Document (ATBD) for Precise Pointing Determination (PPD)
c) Interface Control Document (ICD) for Precise Orbit Determination (POD)
d) Interface Control Document (ICD) Between the Science Investigator-led Processing System (SIPS) and Precision Orbit Determination (POD)/Precision Pointing Determination (PPD) – ICESat-2-SIPS-IFACE-1636
e) Mission Operation Center (MOC) Interface Control Document - 6145330000R0_A%2CMOCICD%2CCDRLMOCMO-2.pdf
f) ASAS Software Design Description Document ICESat-2-SIPS-SPEC-1621 (ATL02 File Format Definition)
g) ICESAT-2 Mission Operations Concept Document ICESAT-2-SYS-PLAN-0006 Algorithm Theoretical Basis Document (ATBD) for ATL03a Atmospheric Delay Correction to Laser Altimetry Ranges

2.0 GENERAL PHOTON EVENT GEOLOCATION ALGORITHM

This section provides a generalized mathematical discussion of the rigorous geolocation of a spaceborne laser altimeter photon event, properly computing the transmit range from the round trip range. The discourse covers the computation of the planet referenced location of the laser altimeter return or bounce point where the laser pointing, S/C attitude, S/C position, and instrument range and timing biases are known and simply combined along with the observed instrument range. The location of the bounce point can be commonly described in terms of geodetic latitude, longitude, and height above a reference ellipsoid or it can be represented in Cartesian coordinates in an Earth Centered Inertial (ECI) or Earth Centered Fixed (ECF) reference frame.

The algorithms used to improve the geolocation through the simultaneous estimation of instrument position, pointing and timing biases from the reduction of altimeter range and S/C tracking data are provided in the *POD, Orbit Design and Geolocation Parameter Calibration ATBD*. The sources and form of input data and the exact implementation of the algorithms for the ICESat-2 mission are discussed in Section 3. Moreover, several simplifying assumptions are made in the ICESat-2 implementation for the purposes of computational efficiency and facilitating post-process analysis, and these are also discussed in Section 3. The only implementation details included in this section are those necessary to clarify the discussion.

2.1 Generalized Input

The geolocation of the photon event bounce point utilizes the following input:

- The round trip range observed by ATLAS

$$o = c\Delta t \quad (2.1.1)$$

$$\Delta t = T_R - T_T \quad (2.1.2)$$

Where

c is the speed of light

T_R is the receive time of the photon

T_T is the transmit time of the laser pulse

1. The laser pulse transmit time and photon receive time are easily related:

$$T_T = T_R - \frac{o}{c} \quad (2.1.3)$$

2. Position and Velocity of the spacecraft (S/C) center of mass in the ECI at T_T

$$\vec{X}^{\,T}_{S/C},\ \vec{V}^{\,T}_{S/C} \quad (2.1.4)$$

- Spacecraft attitude described as the rotation from the Spacecraft Body Fixed frame (SBF) to the ECI at T_T

$$R^T_{SBF\rightarrow ECI} \quad (2.1.5)$$

- Laser altimeter pointing described as a unit vector in the ECI at T_T

$$\hat{u} = R^T_{Laser\rightarrow ECI}\hat{L}^T_{Laser} \quad (2.1.6)$$

Where

$R^T_{Laser\rightarrow ECI}$ is the rotation from the laser frame to the ECI at T_T

$\hat{L}^T_{Laser}$ are the laser beam unit vectors for a spot in the laser frame at T_T

- The pointing vector is then modified to take into account the spacecraft velocity in ECI (velocity aberration). For a satellite velocity of 7 km/s the change in pointing angle is approximately 4.8 arcsec or ~12 m along-track on the Earth's surface from 500 km altitude (from evaluating 2.1.7 using the ICESat-2 End To End Simulator (E2ESim) version 1.0).

$$\hat{p} = \frac{c\hat{u} + \vec{V}^T_{s/c}}{|c\hat{u} + \vec{V}^T_{s/c}|} \quad (2.1.7)$$

- Laser and detector optical offset, or zero range point, from the S/C center of mass in the ECI at T_T and T_R respectively:

$$\vec{x}^T_{cmoff} = R^T_{SBF\rightarrow ECI}\left[\vec{s}^T_{loff} - \vec{s}^T_{cm}\right] \quad (2.1.8)$$

$$\vec{x}^R_{cmoff} = R^R_{SBF\rightarrow ECI}\left[\vec{s}^R_{doff} - \vec{s}^R_{cm}\right] \quad (2.1.9)$$

Where

$\vec{s}^T_{cm}$ is the center of mass vector from the SBF origin in the SBF frame at T_T

$\vec{s}^T_{loff}$ is the laser optical offset vector from the SBF origin in the SBF frame at T_T

$\vec{s}^T_{doff}$ is the detector optical offset vector from the SBF origin in the SBF frame at T_R

2.2 Preliminary Computations

Given the above (Section 2.1), the computation of the photon event bounce point location follows.

- In order to compute the location of the bounce point it is necessary to know the path delay due to atmospheric refraction. However, in order to compute the path delay, the bounce point location is needed. Computing the path delay at an approximate bounce point location solves this problem. The midpoint of the observed two-way range (o) corrected for range biases is used as the approximate location. The error incurred is less than 1 m at 5° off-pointing, which is sufficient to compute the atmospheric refraction delay to sub-mm accuracy (1 m in height is roughly 0.25 mm in path delay, see Section 4.1)

Approximate bounce point location for atmospheric refraction delay computation:

$$\vec{X}^B_{BPapprox} = \vec{X}^T_{S/C} + \vec{x}^T_{cmoff} + \rho \cdot \hat{p} \qquad \rho = \frac{\mathrm{o} - \mathrm{o}_{Ibias}}{2} \quad (2.2.1)$$

Where

o_{Ibias} is the 2-way instrument range bias

Given the above, the atmospheric refraction model can be evaluated for the bounce point in question and a range correction can be computed. See ATL03a Atmospheric Refraction Path Delay ATBD for details of the atmospheric correction computations.

The corrected one-way observation is then computed:

$$\rho_{corr} = \rho - \Delta\rho_{atmref} \quad (2.2.2)$$

Where

ρ_{corr} is the corrected 1-way range observation

$\Delta\rho_{atmref}$ is the atmospheric refraction path delay

- Now, the receive time is computed using the observed range corrected for instrument biases:

$$T_R = T_T + \frac{2\rho}{c} \quad (2.2.3)$$

The S/C center of mass, in the ECI, is then computed at T_R

$$\vec{X}^R_{S/C} \quad (2.2.4)$$

2.3 Light Time Solution for Bounce Point

The altimeter measures a round trip (two-way) range from the laser to the Earth and back again to the detector. During this round trip (~3.2ms for ICESat-2) the S/C position changes appreciably. The effect of this change in position causes the two legs of the altimeter round trip to be unequal. Therefore, we rigorously reconstruct the entire path of the two-way range. This

enables the accurate computation of both the time tag of the bounce point and the 1-way range from the satellite at transmit time to the bounce point, which is necessary for the geolocation computation. The following outlines this procedure:

- The laser and detector zero range points are used as computed above assuming the center of mass offset is slowly varying.

- Consider a triangle formed by each leg of the round trip range and the line connecting the laser and detector optical centers at T_T and T_R. Using the law of cosines we can write an expression for the total round trip range as a function of the transmit leg range. Then an iterative procedure is used to solve for a scale factor which, when multiplied by one half the corrected observation, gives the transmit range.

$$|\vec{x}^R|^2 = |\vec{x}^{TR}|^2 + |\vec{x}^T|^2 - 2(\vec{x}^{TR} \cdot \vec{x}^T) \quad (2.3.1)$$

$$\vec{x}^T = \rho_{corr}^T \cdot \hat{p} \quad (2.3.2)$$

$$\vec{x}^{TR} = \left[\vec{X}_{S/C}^R + \vec{x}_{cmoff}^R\right] - \left[\vec{X}_{\mathrm{S/C}}^T + \vec{x}_{cmoff}^T\right] \quad (2.3.3)$$

- Now, the round trip corrected observation can be expressed as:

$$\rho_{corr}^T + \rho_{corr}^R = \rho_{corr}^T + [|\vec{x}^{TR}|^2 + (\rho_{corr}^T)^2 - 2\rho_{corr}^T(\vec{x}^{TR} \cdot \hat{p})]^{\frac{1}{2}} \quad (2.3.4)$$

- The total round trip corrected range is expressed with the corrected one-way range multiplied by a scale factor:

$$\rho_{corr}^T = s\rho_{corr} \quad (2.3.5)$$

$$Total(s) = s\rho_{corr} + [|\vec{x}^{TR}|^2 + (s\rho_{corr})^2 - 2s\rho_{corr}(\vec{x}^{TR} \cdot \hat{p})]^{\frac{1}{2}} \quad (2.3.6)$$

- Therefore, the corrected transmit leg range may be computed by estimating *s*.

The iterative procedure below is performed to estimate *s*:

1. First iteration, $i = 1$ and guess $s(1) = 1$
2. Evaluate $\varepsilon(i)$:

$$\varepsilon(1) = 2\rho_{corr} - Total\big(s(1)\big) \quad (2.3.7)$$

3. Evaluate $\varepsilon(i), for\ i = 2$ and guess $s(2) = 0.99$
4. Compute gradient ∇f

$$\nabla f = \frac{(\varepsilon(i) - \varepsilon(i-1))}{(s(i) - s(i-1))} \quad (2.3.8)$$

5. Update *s:*

$$s(i+1) = s(i) + \Delta s(i), \quad \Delta s(i) = \frac{-\varepsilon(i)}{\nabla f} \qquad (2.3.9)$$

6. If $\varepsilon(i+1) \leq 1mm$, then the solution has converged. If not converged, repeat steps 4-6.

7. After convergence the transmit leg range is: $\rho_{corr}^{T} = s'\rho_{corr}$ (2.3.10)

2.4 Computation of Bounce Point Location in ECI and Time Tag

The bounce point ECI location and time tag are necessary to compute the location of the bounce point in the Earth Centered Fixed frame (ECF), and to correct this bounce point for time varying effects such as Earth tides, ocean tides, and ocean loading.

- The bounce point location in ECI can be rigorously computed using the converged transmit leg range computed above:

$$\vec{X}_{B(ECI)}^{B} = \vec{X}_{S/C}^{T} + \vec{x}_{cmoff}^{T} + s'\rho_{corr} \cdot \hat{\rho} \quad (2.4.1)$$

- The bounce point time must be computed with the uncorrected transmit leg range:

$$T_B = T_T + s' \frac{\rho}{c} \quad (2.4.2)$$

2.5 Computation of ECF Time Specific Bounce Point Location

- The ECI bounce point position is then rotated to ECF coordinates using the rotations due to precession (P), nutation (N), the Earth's spin (R) and polar motion (W) at the bounce point time (see Section 3 for details):

$$\vec{X}_{B(ECF)}^{B} = W(T_B)R(T_B)N(T_B)P(T_B)\vec{X}_{B(ECI)}^{B} \quad (2.5.1)$$

- Once the ECF bounce point position is computed the time varying surface displacement effects (e.g. solid Earth and ocean tides) at T_B can be evaluated and removed (ATL03 ATBD, Section 6.0, Geophysical Corrections).

2.6 Computation of Geodetic Coordinates

Finally, it is desired to represent the location of the bounce point in a spherical coordinate system defined by an ellipsoid of revolution representing the general geometric shape of the Earth. The ECF bounce point position is then transformed to geodetic coordinates of latitude, longitude and height above the reference ellipsoid. The algorithm can be found in Section 3.2.

3.0 ICESAT-2 IMPLEMENTATION

In this section the specific details of the ICESat-2 received photon geolocation are presented. These details include the specific input and output products, time systems and reference frame details, as well as approximations to both simplify computations and to better facilitate post-geolocation analysis and correction.

3.1 Approximate Geolocation Algorithm

Section 2.1 – 2.5 presented a mathematical treatment for the rigorous geolocation of a received photon. This treatment included the light time solution for the bounce point where the transmit range is specifically computed from the round trip range measured by the altimeter (Section 2.3). In addition, the algorithm corrected the range for atmospheric path delay before the final steps of the geolocation. In the following ICESat-2 implementation the geolocation is performed with an approximate algorithm which negates the need to compute the transmit range from the round trip range for the purposes of geolocation only (not for altimeter measurement modeling for cal/val). Further, the atmospheric refraction path delay is applied after the geolocation to correct the surface bounce point position rather than applied to the altimeter range during the geolocation as in Section 2.2. This is to facilitate the correction and application of a new path delay without having to recompute the geolocation.

What follows is a step-by-step algorithm for geolocating the received photons. All the input parameters for the received photon geolocation algorithm for this step-by-step algorithm are defined in Table 3.1. The source of the input parameters is defined in the Source data column and includes the reference document of the source, where applicable. All the calculated output parameters for the received photon geolocation algorithm are defined in Table 3.2. Table 3.3 provides the geolocation error input and output parameters computed in Section 3.6. It is assumed that the actually coded implementation will efficiently implement this algorithm to work over a logical vector of received photons or a "group" of received photons in time order approximately 5 milliseconds in length or ~40m along-track. The choice of this length is important and depends on the magnitude of the change of the atmospheric path delay and the laser beam pointing over this group length (see equation 3.1.12).

Table 3-1 Input Parameters for the Received Photon Geolocation Algorithm

Value	Units	Description	Variable	Source/Reference Document (Section)
For Section 3.1 Approximate Geolocation Algorithm				
Number of photons		Number of photons in group	N	ATL02_yyyydddssss_vVV / SIPS ATL02 Format Def
Photon index		The *i*th photon in group	i	
Reference photon		The *j*th photon in	j	From signal finding algorithm

Value	Units	Description	Variable	Source/Reference Document (Section)
For Section 3.1 Approximate Geolocation Algorithm				
index		group		
Time of flight observation	sec	Receive photon time of flight observation for the i photon in group (Eq. 3.1.1)	$tof(i)$	ATL02_yyyydddssss_vVV / SIPS ATL02 Format Def
Received photon transmit time	sec	Laser pulse start time in GPS time (Eq. 3.1.1)	t_T	ATL02_yyyydddssss_vVV / SIPS ATL02 Format Def
Range bias which includes static and time varying ZRP.	sec	From ISF ZRB file and computed from POD Instrument cal/val analysis (Eq. 3.1.2)	ρ_{bias}	ANC04_p_yyyydddssss_vVV / POD Facility ICD ICESat-2-FOPS-IFACE-4736 (4.4.3, 5.2.1)
1-way average range	m	1-way range corrected for the range bias (Eq. 3.1.2)	ρ	Calculated
Speed of light	m/sec	Constant (Eq. 3.1.3)	c	Section 4.5 Observables, Models, Constants and Standards / POD ATBD (1.2.2a)
LF to ECI rotation		Laser Frame, LF (LRS laser-side) rotation (Eq. 3.1.5)	$R_{LF \rightarrow ECI}$	ANC05_p_yyyydddssss_vVV / POD Facility ICD ICESat-2-FOPS-IFACE-4736 (4.4.3, 5.2.1)
Center of mass offset	m	Provided from MOC to POD and computed from a tuned model as a function of solar array azimuth and elevation. Rotated into LF frame and provided in ANC04 (Eq. 3.1.5)	$\vec{s}_{cm}$	ANC04_p_yyyydddssss_vVV_cal / POD Facility ICD ICESat-2-FOPS-IFACE-4736 (4.4.3, 5.2.1)
Atlas DOE point	m	From coordinate systems document, rotated into LF frame and provided in ANC04 (Eq.3.1.5)	$\vec{s}_{DOE}$	ANC04_p_yyyydddssss_vVV / POD Facility ICD ICESat-2-FOPS-IFACE-4736 (4.4.3, 5.2.1)
S/C center of mass position	m	Computed at bounce time by interpolating the daily precision orbit ephemeris in ECI	$\vec{X}_{s/c}$	ANC04_p_yyyydddssss_vVV / POD Facility ICD ICESat-2-FOPS-IFACE-4736 (4.4.3, 5.2.1)

Value	Units	Description	Variable	Source/Reference Document (Section)
For Section 3.1 Approximate Geolocation Algorithm				
		frame (Eq. 3.1.6)		
S/C center of mass velocity	m/sec	Computed at bounce time by interpolating the daily precision orbit ephemeris in ECI frame (Eq. 3.1.6)	$\vec{V}_{s/c}$	ANC04_p_yyyydddssss_vVV / POD Facility ICD ICESat-2-FOPS-IFACE-4736 (4.4.3, 5.2.1)
Pointing unit vector in inertial frame (ECI)	Unit vector	Calibrated for each spot (Eq. 3.1.7)	$\hat{L}_{ECI}$	ANC05_p_yyyydddssss_vVV_cal / POD Facility ICD ICESat-2-FOPS-IFACE-4736 (4.4.3, 5.2.1)
ECI to ECF quaternions		Interpolated from ECI to ECF daily quaternions (Eq. 3.1.9)	$R_{ECI \rightarrow ECF}$	ANC03_p_yyyydddssss_vVV/ POD Facility ICESat-2-FOPS-IFACE-4736 (4.4.3, 5.2.1)
For Section 3.2 Computing geodetic spherical coordinates referenced to the ellipsoid from ECF Cartesian Coordinates				
Semi-major axis	m	Semi-major axis of the adopted Earth ellipsoid (section 3.2)	a_e	Section 6.0 Geophysical Corrections / ATL03 (1.2.1b)
Semi-minor axis	m	Semi-minor axis of the adopted Earth ellipsoid (section 3.2)	b_e	Section 6.0 Geophysical Corrections / ATL03 (1.2.1b)
Flattening		Flattening of the adopted Earth ellipsoid (section 3.2)	f	Section 6.0 Geophysical Corrections / ATL03 (1.2.1b)

Table 3-2 Calculated Output Parameters for Received Photon Geolocation Algorithm

Algorithm: only needed internally for the algorithm per photon group **Geolocation: the geolocation output parameters to be retained in the ATL03 product**				
Value	**Units**	**Description**	**Variable**	**Target Output**
Corrected receive times for all photons in the group	sec	Calculated from the receive photon transmit time and round trip range corrected for range bias (Eq. 3.1.3)	$t_R(i)$	Algorithm
Bounce point times for all photons in the group.	sec	Calculated from the received photon transmit time and the 1-way range corrected for range bias (Eq. 3.1.4)	$t_B(i)$	**Geolocation**

Algorithm: only needed internally for the algorithm per photon group **Geolocation: the geolocation output parameters to be retained in the ATL03 product**				
Value	**Units**	**Description**	**Variable**	**Target Output**
Instrument DOE offset vector in ECI	m	Calculated at transmit time from zero range point and center of mass vectors in LF and transformed with ECI rotation (Eq. 3.1.5)	$\vec{x}_{DOEoff}$	Algorithm
Transmit pointing vector in ECI	Unit vector	Computed at transmit time by Eq. 3.1.7	$\hat{p}$	Algorithm
Bounce point location in ECI	m	Computed from Eq. 3.1.8	$\vec{B}_{ECI}$	Algorithm
Bounce point location in ECF	m	Rotated to ECF by interpolating the daily ECI to ECF quaternions (Eq. 3.1.9)	$\vec{B}_{ECF}$	Algorithm
Geodetic latitude of bounce points	degree	Computed from ECF using section 3.2 algorithm for all photons in the group.	$\phi(i)$	Algorithm
East longitude of bounce points	degree	Computed from ECF using section 3.2 algorithm for all photons in the group.	$\lambda(i)$	Algorithm
Ellipsoid height of bounce points	m	Computed from ECF using section 3.2 algorithm for all photons in the group.	$h(i)$	Algorithm
Index *j* for the received photon	integer	Index *j* from the group of geolocated received photons that is closest to the middle of the time period and nearest to the mean of the signal photons (Section 3.1 Step 8)	j	**Geolocation**
Unit pointing vector in ECF for the reference photon	Unit vector	Unit pointing vector in ECF for the reference photon (Eq. 3.1.10).	$\hat{u}(j)$	Algorithm

Algorithm: only needed internally for the algorithm per photon group **Geolocation: the geolocation output parameters to be retained in the ATL03 product**				
Value	**Units**	**Description**	**Variable**	**Target Output**
Azimuth of the unit pointing vector for the reference photon	radian	Azimuth of the unit pointing vector for the reference photon in the local ENU frame in radians. The angle is measured from North and positive towards East. (Section 3.3 algorithm)	$ref\_azimuth(j)$	**Geolocation**
Elevation of the unit pointing vector for the reference photon	radian	Elevation of the unit pointing vector for the reference photon in the local ENU frame in radians. The angle is measured from East-North plane and positive towards Up. (Section 3.3 algorithm)	$ref\_elev(j)$	**Geolcation**
Azimuth of the Sun position vector from the reference photon bounce point position	radian	Azimuth of the Sun position vector from the reference photon bounce point position in the local ENU frame in radians. The angle is measured from North and positive towards East. (Section 3.3 algorithm)	$solar\_azimuth(j)$	**Geolocation**
Elevation of the Sun position vector from the reference photon bounce point position	radian	Elevation of the Sun position vector from the reference photon bounce point position in the local ENU frame in radians. The angle is measured from East-North plane and positive towards Up. (Section 3.3 algorithm)	$solar\_elevation(j)$	**Geolcation**
Atmospheric path delay in range for the reference photon	m	Calculated using the ATL03a algorithm for the reference photon	$\rho_{atm}(j)$	**Geolocation**
Atmospheric path delay derivative with respect to ellipsoid height	m/m	Calculated using the ATL03a algorithm for the reference photon	$\frac{\partial \rho_{atm}(j)}{\partial h(j)}$	**Geolocation**
Atmospheric path delay in range for all photons in the group	m	Calculated from the *j* reference photon path delay, derivative and height, and the *i* photons in the group (Eq. 3.1.11)	$\rho_{atm}(i)$	Algorithm

Algorithm: only needed internally for the algorithm per photon group **Geolocation: the geolocation output parameters to be retained in the ATL03 product**				
Value	**Units**	**Description**	**Variable**	**Target Output**
Bounce point in ECF corrected for atmospheric path delay for all received photons in the group	m	Calculated using the ECF bounce points and the atmospheric path delay for all photons in the group and the ECF unit pointing vector for the reference photon (Eq. 3.1.12)	$\vec{B}_{ECF}^{'}(i)$	Algorithm
Geodetic latitude of bounce points corrected for atmospheric path delay	degree*	Computed from ECF bounce points using section 3.2 algorithm for all photons in the group	$\phi'(i)$	**Geolocation**
East longitude of bounce points corrected for atmospheric path delay	degree*	Computed from ECF bounce points using section 3.2 algorithm for all photons in the group	$\lambda'(i)$	**Geolocation**
Ellipsoid height of bounce points corrected for atmospheric path delay	m	Computed from ECF bounce points using section 3.2 algorithm for all photons in the group	$h'(i)$	**Geolocation**
***Note: when using these variables in the equations in this document ensure the units are in radians.**				

Table 3-3 Geolocation Error Input and Output Parameters

Input: Needed to compute geolocation error uncertainty **Output: Geolocation output error uncertainties computed in Section 3.6**				
Value	**Units**	**Description**	**Variable**	**Target / Source**
Position 1-σ error estimate	m	1-σ position uncertainty estimates in RIC frame	$\delta\vec{X}_{S/C}^{\sigma}$	Input / ANC04_p_yyyydddssss_vVV
Range 1-σ error estimate	m	1-σ uncertainty in receive photon 1-way range measurement	$\delta\rho^{\sigma}$	Input / ANC04_p_yyyydddssss_vVV
Pointing 1-σ error estimate		1-σ uncertainty rotations of the laser pointing vectors	$\delta\alpha^{\sigma}$	Input / ANC05_p_yyyydddssss_vVV

Input: Needed to compute geolocation error uncertainty **Output: Geolocation output error uncertainties computed in Section 3.6**				
Value	**Units**	**Description**	**Variable**	**Target / Source**
Geodetic latitude 1-σ error estimate	degree	Geodetic latitude 1-σ uncertainty of the reference photon bounce point	$\Delta\phi(j)$	Output
East longitude 1-σ error estimate	degree	East longitude 1-σ uncertainty of the reference photon bounce point	$\Delta\lambda(j)$	Output
Ellipsoid height 1-σ error estimate	m	Ellipsoid height 1-σ uncertainty of the reference photon bounce point	$\Delta h(j)$	Output
Sigma_along 1-σ error estimate	m	Estimated uncertainty for the reference photon bounce point along-track component: 1-σ	$Sigma\_along$	Output
Sigma_across 1-σ error estimate	m	Estimated uncertainty for the reference photon bounce point cross-track component: 1-σ	$Sigma\_across$	Output

STEP 1: range observations and time tags

A "group" of N receive photon transmit times and time-of-flight (*tof*) observations are obtained from ATL02, and a 1-way average range corrected for a range bias is computed. The range bias is obtained from the POD Instrument Cal/Val team's analysis of the ISF Zero Range Bias (ZRB) file, and is supplied in the ANC04_p_yyyydddsssss_vVV file (see ICD for POD ICESat-2-FOPS-IFACE-4736) for each specific beam. The range bias is measured from the ATLAS Diffractive Optical Element point (DOE) and includes the constant Zero Range Point (ZRP) correction as well as the time varying ZRP correction. The range bias needs to be interpolated to the time of transmit for each photon. The range bias is dependent on the hardware configuration, which includes the start pulse detector (A or B), the receive photon detector (A or B), and the laser (1 or 2). The current hardware configuration is supplied in the ISF ZRB file and the configuration is then provided in the ANC04_p_yyyydddsssss_vVV file.

$$i = 1 \rightarrow N\ photons \qquad tof(i), t_T(i) \qquad (3.1.1)$$

$$\rho(i) = \frac{tof(i)}{2} * c \quad - \quad \rho_{bias}\left(t_T(i)\right) \quad (3.1.2)$$

Which is:

$$\rho(i) = \rho_{obs}(i) \quad - \quad \rho_{bias}\left(t_T(i)\right)$$

Corrected receive time is then computed:

$$t_R(i) = \ t_T(i) + \frac{2\rho(i)}{c} \qquad (3.1.3)$$

The approximate bounce point time is computed:

$$t_B(i) = t_T(i) + \frac{\rho(i)}{c} \qquad (3.1.4)$$

STEP 2: center of mass to instrument tracking point vector (DOE) and accounting for ZRP.

The ATLAS Diffractive Optical Element point (DOE) is a known point that all beams pass through. It is a fixed position in the Master Reference Frame (MRF) and is used as the instrument tracking point for the geolocation computations. The vector from the observatory center of mass to the ATLAS DOE is computed at transmit time in a common frame (LF), and then rotated to the ECI frame. The ATLAS DOE vector is supplied in the ANC04_p_yyyydddssssss_vVV POD product and is assumed to be static (time invariant). The vector from the DOE to the time varying ZRP is accounted for by applying the range bias in 3.1.2 (with 3.1.8, it is then algebraically equivalent to applying the ZRP vector as the range correction is the ZRP range correction applied along the anti-pointing vector). The offset vector for the center of mass is computed from two elements: Mission notification products supplied by the MOC to POD noting the change in the vector after orbit maneuver burns, and a tuned model of the center of mass variation as a function of solar array azimuth and elevation (see Table 3.1; ICESat2_Manuever_Log.txt, ICESat2_COM_*yyyy-ddd-hhmmss*.txt) are used to produce a time varying center of mass vector that is provided in the ANC04_p_yyyydddssssss_vVV POD product. The LF to ECI rotation is provided in the ANC05_p_yyyydddssssss_vVV_cal POD product and is computed from the star frame to J2000 quaternions provided as a PPD product and the calibrated star frame to laser frame quaternions provided by POD (see POD Facility ICD ICESat-2-FOPS-IFACE-4736). See section 3.5 concerning a note about interpolation.

$$\vec{x}_{\ DOEoff}(i) = R_{LF \to ECI}\left(t_T(i)\right)\left[\vec{s}_{DOE} - \vec{s}_{cm}\left(t_T(i)\right)\right] \quad (3.1.5)$$

STEP 3: spacecraft center of mass position and velocity in the ECI frame

The spacecraft center of mass ECI position and velocity are computed at the bounce time by interpolating the daily ANC04_p_yyyydddsssss_vVV precision orbit ephemeris file (see POD Facility ICD ICESat-2-FOPS-IFACE-4736). See section 3.5 concerning a note about interpolation.

$$\vec{X}_{s/c}\left(t_B(i)\right), \qquad \vec{V}_{s/c}\left(t_B(i)\right) \qquad (3.1.6)$$

STEP 4: transmit pointing vector in ECI frame

The ECI laser beam pointing unit vector for each spot is computed at transmit time interpolating the following data set for each spot:

ANC05_p_yyyydddsssss_vVV_cal – pointing unit vector in ECI frame calibrated for each spot

$$\hat{p}(i) = \hat{L}_{ECI}\left(t_T(i)\right) \quad (3.1.7)$$

STEP 5: bounce point ECI Cartesian coordinates

The bounce point ECI Cartesian coordinates are computed as follows:

$$\vec{B}_{ECI}(i) = \vec{X}_{s/c}\left(t_B(i)\right) + \vec{x}_{\,DOEoff}(i) + \rho(i) \cdot \hat{p}(i) \qquad (3.1.8)$$

To be thorough, we now show that the above equation takes into account the time varying ZRP vector. The corrected range can be represented as a sum of the observed range and the range

$$\vec{B}_{ECI}(i) = \vec{X}_{s/c}\left(t_B(i)\right) + \vec{x}_{\,DOEoff}(i) + \rho_{obs}(i) \cdot \hat{p}(i) - \rho_{bias}\left(t_T(i)\right) \cdot \hat{p}(i)$$

$$\vec{x}_{ZRP}(i) = \vec{x}_{\,DOEoff}(i) - \rho_{bias}\left(t_T(i)\right) \cdot \hat{p}(i)$$

Which gives:

$$\vec{B}_{ECI}(i) = \vec{X}_{s/c}\left(t_B(i)\right) + \vec{x}_{\,ZRP}(i) + \rho_{obs}(i) \cdot \hat{p}(i)$$

STEP 6: bounce point ECF Cartesian coordinates

The bounce point ECI Cartesian coordinates are then rotated to ECF interpolating the daily ECI to ECF ANC03_p_yyyydddsssss_vVV quaternion files:

$$\vec{B}_{ECF}(i) = R_{ECI \to ECF}\left(t_B(i)\right) \vec{B}_{ECI}(i) \quad (3.1.9)$$

Equation 3.1.8 is an approximation to the geolocation algorithm presented in Section 2 which performs the light time solution to compute the transmit range. Equation 3.1.8 uses the instrument ZRP and pointing vector evaluated at transmit time as in the rigorous geolocation algorithm. However, equation 3.1.8 uses the spacecraft center of mass position evaluated at the

bounce time as well as the 1-way range instead of the true transmit leg range. It should also be noted that velocity aberration is not applied as in the rigorous geolocation algorithm. The ICESat-2 maximum spacecraft motion is approximately 5 cm in altitude and approximately 12.6 m along-track over 1-way photon travel time or approximately 1.6 milliseconds. The total position change of the spacecraft from transmit time to bounce time compensates for the range difference between the simple 1-way range and actual transmit leg range, and provides the along-track shift equivalent to velocity aberration. This approximate geolocation algorithm has been shown to be accurate to a few tenths of a millimeter in total bounce point position during nominal reference ground track mapping and 5° scan maneuvers. While this approximation serves the purposes of receive photon geolocation well, the rigorous light time solution of the transmit leg range is employed in the direct altimetry and dynamic crossover measurement modeling used for instrument parameter calibration from altimeter range residual analysis (see the *POD, Orbit Design and Geolocation Parameter Calibration ATBD*).

STEP 7: initial bounce point latitude, longitude and height computation

The ECF bounce points computed in 3.1.9 are then converted to a geodetic spherical coordinate system relative to the reference ellipsoid using the algorithm defined in section 3.2.

Input to the section 3.2 algorithm: the array of ECF bounce points for the *N* photons: $\vec{B}_{ECF}(i)$

Output from the section 3.2 algorithm: the following arrays for the *N* photons:

$\phi(i)$ is the geodetic latitude, the acute angle between the semi-major axis and a line through the observer perpendicular to the spheroid

$\lambda(i)$ is the east longitude, the angle measured eastward in the equatorial plane between the Greenwich meridian and the observer's meridian

$h(i)$ is the ellipsoid height, the perpendicular height above the reference ellipsoid

*Note: WGS84 ellipsoid should be used as the ATL03a algorithm expects the geodetic spherical coordinates to be referenced to WGS84. Geodetic latitude and longitude are output in units of degrees for ALT03g, but they must be used with units of radians in the equations presented this document.

STEP 8: Finding the reference signal photon

The *N* geodetic spherical coordinates computed in step 7, as well as the 1-way ranges for all the photons in the group, are then passed to the signal finding algorithm that returns the index *j* for the received photon that is closest to the middle of the time period and nearest to the mean of the signal photons.

Signal finding algorithm input: $\phi(i),\ \lambda(i),\ h(i),\ \rho(i)$

Signal finding algorithm output: the index *j* identifying which of the *N* received photons that is closest to the middle of the time period and nearest to the mean of the signal photons

* Here it is assumed that the surface mask look up is part of the signal finding algorithm.

STEP 9: Correcting the bounce point ECF Cartesian coordinates for atmospheric refraction path delay correction

Another important aspect of the approximate geolocation algorithm is the 1-way range used in the computations has not been corrected for atmospheric refraction path delay. The 1-way range can easily be corrected for the path delay in equation 3.1.2. However, doing so does not allow changing the path delay correction after the geolocation in a case where one wishes to apply a new path delay model or atmospheric model. Therefore, the ICESat-2 implementation corrects the bounce point ECI Cartesian coordinates for the path delay after the bounce point computation with the following algorithm. In addition, the path delay and its derivative with respect to ellipsoid height are computed for the reference signal photon and used to correct all other photons in the group in order to conserve storage and computational resources.

The path delay and its derivative with respect to the ellipsoid height of the bounce point are then computed for the reference photon, which has been identified as the j^{th} received photon (see ATL03a Atmospheric Delay Correction ATBD). The ECI pointing vector from the geolocation computation is retained for the j^{th} received photon in the group and rotated to ECF.

First, the unit pointing vector in the ECF is computed for the reference photon:

$$\hat{u}(j) = -R_{ECI \rightarrow ECF}(t_B(j))\, \hat{p}(j) \qquad (3.1.10)$$

Then azimuth and elevation are computed in a local East, North and Up (ENU) reference frame for the reference photon using the algorithm in section 3.3.

Input to the section 3.3 algorithm:

$\hat{u}(j)$ is the unit pointing vector for the reference photon in ECF.

$\phi(j),\ \lambda(j)$ geodetic latitude and longitude for the reference photon.

Output from the section 3.3 algorithm:

$ref\_azimuth(j)$ is the azimuth of the unit pointing vector for the reference photon in the local ENU frame in radians. The angle is measured from North and positive towards East.

$ref\_elev(j)$ is the elevation of the unit pointing vector for the reference photon in the local ENU frame in radians. The angle is measured from East-North plane and positive towards Up.

The path delay and its derivative with respect to the ellipsoid height of the bounce point are then computed for the reference photon using the algorithm in ATL03a.

Input to ATL03a algorithm:

$$t_B(j), \quad \phi(j), \quad \lambda(j), \quad h(j), \quad ref\_azimuth(j), \quad ref\_elev(j)$$

$t_B(j)$ should be passed to the ATL03a algorithm as elapsed seconds from a reference epoch given in GPS time.

*Note: WGS84 ellipsoid should be used as the ATL03a algorithm expects the geodetic spherical coordinates to be referenced to WGS84.

Output from ATL03a algorithm:

$$\rho_{atm}(j), \qquad \frac{\partial \rho_{atm}(j)}{\partial h(j)}$$

The bounce point ECF Cartesian coordinates and bounce time for all of the received photons within the group are corrected for atmospheric refraction path delay using the information from equation 3.1.10 and the change in the difference in the ellipsoid height between the i^{th} and j^{th} received photons:

$$\rho_{atm}(i) = \rho_{atm}(j) + \left[\frac{\partial \rho_{atm}(j)}{\partial h(j)} \left(h(i) - h(j)\right)\right] \qquad (3.1.11)$$

$$\vec{B}_{ECF}^{\,\prime}(i) = \vec{B}_{ECF}(i) + \rho_{atm}(i) \cdot \left(\hat{u}(j)\right) \qquad (3.1.12)$$

The corrected ECF bounce points computed in 3.1.12 are then converted to a geodetic spherical coordinate system relative to the reference ellipsoid using the algorithm defined in section 3.2 and the inputs as described in Step 7.

Input to the section 3.2 algorithm: the array of corrected ECF bounce points for the *N* photons:

$$\vec{B}_{ECF}^{\,\prime}(i)$$

Output from the section 3.2 algorithm: are the corrected geodetic latitude, longitude and height above the reference ellipsoid arrays for the *N* photons.

$$\phi'(i), \qquad \lambda'(i), \qquad h'(i)$$

The above are to be retained in the data products as the geolocation along with the *ref_azimuth* and *ref_elev* , atmospheric path delay, and atmospheric path delay derivative for the j^{th} reference photon:

$$j, \qquad ref\_azimuth(j), \qquad ref\_elev(j), \quad \rho_{atm}(j), \qquad \frac{\partial \rho_{atm}(j)}{\partial h(j)}$$

Equation 3.1.11 and 3.1.12 represent sufficient sub-mm approximations for a received photon group length of 40 m along-track on the surface or 5.26 msec in time. The change in the path delay is negligible for 100s of meters of change in the horizontal bounce point position, and the change in the path delay due to a change in the bounce point ellipsoid height is on the order of 0.25 mm per 1 meter, and is modeled by the derivative output from the ATL03a algorithm, which is applicable over the 5.26 msec group. An additional approximation is used in equation 3.1.12 where the pointing vector for the j^{th} received photon transmit time is used to compute the

correction for all of the received photons within the group. The maximum change in the pointing during science operations and scan maneuvers over 2.63 msec is on the order of 3.3 arcseconds in pointing change. This level of pointing change applied to the path delay of ~2 meters results in negligible errors in the corrected bounce point position. Finally, the correction is applied in the ECF without taking into account the rotating frame. However, this is not an issue as the ECF frame is essentially an inertial frame over the ~2 m light time of the path delay.

Note: Section 3.4 provides the algorithm to apply a new atmospheric range correction entirely in geodetic spherical coordinates referenced to the ellipsoid without going back to the ECI or ECF frames or requiring re-computation of the position and pointing vectors.

3.2 Computing geodetic spherical coordinates referenced to the ellipsoid from ECF Cartesian Coordinates

Assumption: h << N, e<<1

The ECF bounce point Cartesian coordinates are converted to geodetic coordinates of latitude, longitude and height above the reference ellipsoid. The reference ellipsoid of the Earth can be uniquely defined by:

a_e is the Earth eccentricity squared is the semi-major axis of the adopted Earth ellipsoid

b_e is the semi-minor axis of the adopted Earth ellipsoid

$f = \frac{a_e - b_e}{a_e}$ is the flattening of the adopted Earth ellipsoid (3.1.13)

$e^2 = 1 - (1 - f)^2$ is the Earth eccentricity squared

The following geodetic coordinates are then computed from the reference ellipsoid:

ϕ is the geodetic latitude, the acute angle between the semi-major axis and a line through the observer perpendicular to the ellipsoid

λ is the east longitude, the angle measured eastward in the equatorial plane between the Greenwich meridian and the observer's meridian

h is the ellipsoid height, the perpendicular height above the reference ellipsoid

The geodetic coordinates are computed from the ECF Cartesian coordinates of the bounce point using the following iterative procedure:

- ECF Cartesian coordinates of the bounce point are expanded in the below equations to be X, Y, Z.
- Make initial estimate for parameter *t:*

$$t \cong e^2 Z$$

- Compute the following quantities on each iteration:

$$Z_t = Z + t$$

$$(N + h) = \sqrt{X^2 + Y^2 + Z_t^2}$$

$$sin\phi = \frac{Z_t}{(\mathrm{N} + \mathrm{h})}$$

$$N = \frac{a_e}{\sqrt{1 - e^2\, sin^2\phi}}$$

$$t = Ne^2 sin\phi$$

- When t converges (sub-mm), the ellipsoid height is the difference of the bounce point distance from the center of curvature and the surface distance from the center of curvature. This is given by:

$$h = (N + h) - N$$

- Geodetic latitude and longitude are then given by:

$$\phi = tan^{-1}\left(\frac{Z_t}{\sqrt{X^2 + Y^2}}\right) \text{ or } sin^{-1}\left(\frac{Z_t}{(N+h)}\right)$$

$$\lambda = \tan^{-1}\left(\frac{Y}{X}\right)$$

- Geodetic latitude and longitude are then converted to have units of degrees: $\frac{180°}{radian}$

3.3 Computing Pointing and Solar vector Azimuth and Elevation in the local ENU Frame

Given geodetic latitude and longitude coordinates *(ϕ, λ)*, the transformation matrix from the Earth Centered Fixed frame into the local East-North-Up (ENU) frame C_{ECF}^{ENU} is given as:

$$C_{ECF}^{ENU} = \begin{bmatrix} -sin\lambda & cos\lambda & 0 \\ -cos\lambda sin\phi & -sin\lambda sin\phi & cos\phi \\ cos\lambda cos\phi & sin\lambda cos\phi & sin\phi \end{bmatrix}$$

Then the local East-North-Up (ENU) pointing unit vector $\begin{bmatrix} u_e \\ u_n \\ u_{up} \end{bmatrix}$ is computed as:

$$\begin{bmatrix} u_e \\ u_n \\ u_{up} \end{bmatrix} = C_{ECF}^{ENU}\,\hat{u}(j)$$

Where $\hat{u}(j)$ is the Earth Centered Fixed pointing unit vector of the j^{th} reference photon.

Using East-North-Up unit vector, the azimuth and elevation are given by:

$$ref\_elev = \sin^{-1}(\hat{u}_{up}), \qquad -{}^{\pi}/_{2} \le El \le {}^{\pi}/_{2}$$

$$ref\_azimuth = \tan^{-1}\left(\frac{\hat{u}_e}{\hat{u}_n}\right), \qquad -\pi \le Az \le \pi$$

The Sun position ENU orientation angles (*solar_azimuth, solar_elevation*) relative to the reference photon bounce point position are also output parameters of the geolocation algorithm. The following equations are found in the reference *Fundamentals of Astrodynamics and Applications, 2nd Edition, David A*. Vallado, and follow the mathematical algorithm from the *Astronomical Almanac* (1992, C24) to produce a J2000 Sun position vector with accuracy of 0.01^o.

We need to start by computing the Sun position vector, $\vec{r}_{\odot}$ at the reference photon bounce time, $t_B(j)$. The algorithm takes as input this time given as UT1 Julian Date. The time is expressed as Julian centuries:

$$T_{UT1} = \frac{JD_{UT1} - 2{,}451{,}545.0}{36{,}525}$$

Note: If $UT1 - UTC$ isn't readily available, the approximation of $UT1 \approx UTC$ will sacrifice little precision. Also, the algorithm from "Practical Ephemeris Calculations" by Oliver Montenbruck (Springer-Verlag, 1989) converts calendar dates into Julian dates.

The mean longitude of the Sun, $\lambda_{M_{\odot}}$ is computed as:

$$\lambda_{M_{\odot}} = 280.4606184° + 36{,}000.77005361T_{UT1}$$

Using TDB time is precise, but we can sacrifice some precision and set TDB and UT1 times equal,

$$T_{TDB} \approx T_{UT1}$$

The mean anomaly of the Sun, $M_{\odot}$ is computed as:

$$M_{\odot} = 357.5277233° + 35{,}999.05034T_{TDB}$$

Convert $M_{\odot}$ into units of radians using the conversion:

$$1° = \frac{\pi}{180} rad$$

The ecliptic longitude, $\lambda_{ecliptic}$ is computed as:

$$\lambda_{ecliptic} = \lambda_{M_{\odot}} + 1.914666471° \sin M_{\odot} + 0.019994643 \sin 2M_{\odot}$$

The mean obliquity of the ecliptic, ϵ is computed as:

$$\epsilon = 23.439291° - 0.0130042T_{TDB}\ (0 - 2\pi)$$

Convert both $\lambda_{ecliptic}$ and ϵ into units of radians.

The position magnitude of the Sun, $r_{\odot}$ in AU is given as:

$$r_{\odot} = 1.000140612 - 0.016708617 \cos M_{\odot} - 0.000139589 \cos 2M_{\odot}$$

Finally, the position vector of the Sun, $\vec{r}_{\odot}$ in geocentric equatorial coordinates (J2000) is given by:

$$\vec{r}_{\odot} = \begin{bmatrix} r_{\odot} \cos \lambda_{ecliptic} \\ r_{\odot} \cos \epsilon \sin \lambda_{ecliptic} \\ r_{\odot} \cos \epsilon \sin \lambda_{ecliptic} \end{bmatrix} AU$$

Convert $\hat{r}_{\odot}$ to meters with the following conversions:

$$1\ AU = 149{,}597{,}870.7\ km, \qquad 1\ km = 1{,}000\ m$$

Transform the Sun J2000 vector into the ECF frame as:

$$R_{ECI \rightarrow ECF}(t_B(j))\ \vec{r}_{\odot}$$

The Sun vector from the photon bounce point is then calculated as:

$$\hat{u} = \left\| R_{ECI \rightarrow ECF}\left(t_B(j)\right) \vec{r}_{\odot} \ - \ \vec{B}_{ECF}(j) \right\|$$

It should be noted that effects such as atmospheric refraction are not included in this algorithm. Refer back to the beginning of this section to compute solar azimuth (*solar_azimuth*) and elevation (*solar_elevation*) angles from the ECF pointing vector, $\hat{u}$.

3.4 Applying a new atmospheric range correction in geodetic spherical coordinates referenced to the ellipsoid.

Given the geodetic spherical coordinates for a group of N (i goes from 1 to N) bounce points that already have the correction for atmospheric path delay included, as well as the ENU azimuth, elevation, original atmospheric path delay and the derivative of the path delay with respect to ellipsoid height for the j^{th} reference photon:

$$\phi'(i), \qquad \lambda'(i), \qquad h'(i)$$

$$j, \qquad ref\_azimuth(j), \qquad ref\_elev(j), \quad \rho_{atm}(j), \qquad \frac{\partial \rho_{atm}(j)}{\partial h(j)}$$

We can compute new geodetic lat, lon and height for the bounce points given a new atmospheric path delay.

The new atmospheric path delay and derivative are computed for the reference photon:

$$\rho_{Natm}(j), \qquad \frac{\partial \rho_{Natm}(j)}{\partial h(j)}$$

Because the original ellipsoid height uncorrected for atmospheric path delay is not retained, the original atmospheric path delay must be computed using the corrected ellipsoid heights. However, this approximation is valid as the change in the path delay due to a change in ellipsoid height is on the order of 0.25mm per meter, and the difference between the uncorrected delta heights and the corrected delta heights is approximately the difference in the atmospheric path delay over the change in height.

$$\left(h'(i) - h'(j)\right) \approx \left(1 + \frac{\partial \rho_{atm}(j)}{\partial h(j)}\right) \left(h(i) - h(j)\right)$$

$$\left(h'(i) - h'(j)\right) \approx \left(1.00025\ \frac{cm}{m}\right) \left(h(i) - h(j)\right)$$

Recognizing that the delta height is then multiplied by the delta partial of the path delay with respect to the ellipsoid height it is clear that the approximation using the corrected ellipsoid heights imposes a negligible error.

Compute delta atmospheric path delay:

$$\Delta\rho_{atm}\,(i) = \left(\rho_{Natm}\,(j) - \rho_{atm}\,(j)\right) + \left(\frac{\partial\rho_{Natm}\,(j)}{\partial h(j)} - \frac{\partial\rho_{atm}\,(j)}{\partial h(j)}\right)\cdot\left(h'(i) - h'(j)\right)$$

Compute the earth radius at the bounce points using the parameters of the reference ellipsoid:

$$R_E(i) = \sqrt{\frac{(a_E^2\cos(\phi'(i)))^2 + (b_E^2\sin(\phi'(i)))^2}{(a_E\cos(\phi'(i)))^2 + (b_E\sin(\phi'(i)))^2}}$$

Compute the unit pointing vector in the ENU frame from *Az* and *El* for the reference photon:

$$\begin{bmatrix} u_{\hat{e}} \\ u_{\hat{n}} \\ u_{\widehat{up}} \end{bmatrix} = \begin{bmatrix} \cos ref\_elev(j)\sin ref\_azimuth(j) \\ \cos ref\_elev(j)\cos ref\_azimuth(j) \\ \sin ref\_elev(j) \end{bmatrix}$$

This pointing vector is used in the computation for all photons in the group. The maximum change in the pointing during science operations and scan maneuvers over 2.63 msec (40 m along-track group length) is on the order of 3.3 arcseconds in pointing change. This level of pointing change applied to the path delay of ~2 meters results in negligible errors in the corrected bounce point position.

The change in latitude (in radians) due to the change in the atmospheric path delay correction can be expressed in radians as:

$$\Delta\phi(i) = \frac{\Delta\rho_{atm}(i)\,u_{\hat{N}}}{R_E}$$

The change in longitude (in radians) due to the change in the atmospheric path delay correction can be expressed in radians as:

$$\Delta\lambda(i) = \frac{\Delta\rho_{atm}(i)\,u_{\hat{e}}}{R_E\cos\phi}$$

The change in height due to the change in the atmospheric path delay correction can be expressed in meters as:

$$\Delta h(i) = \Delta\rho_{atm}u_{\widehat{up}}$$

Compute new latitude, longitude and height due to the difference between the new and original atmospheric path delay:

$$\phi^N(i) = \phi'(i) + \Delta\phi(i)$$

$$\lambda^N(i) = \lambda'(i) + \Delta\lambda(i)$$
$$h^N(i) = h'(i) + \Delta h(i)$$

Make sure to use consistent units when performing these computations and take note that the output variables in Table 3-2 are in degrees.

3.5 A note about position, velocity and quaternion interpolation

A Hermite 9th or 10th order polynomial interpolation algorithm is recommended for interpolating the spacecraft position and velocity data. The Hermite interpolator has been shown to be both extremely computationally efficient and extremely accurate to sub-micron and sub-micron/s when interpolating a typical LEO ephemeris with 5 – 30 second data postings. The Hermite interpolator naturally provides interpolation of both position and velocity. It is recommended that the algorithm implementer perform a thorough evaluation of the interpolation performance.

A Lagrange 9th order polynomial interpolation has been found to be accurate to 0.002" when interpolating a time series of quaternions with 5 second sampling. It is recommended that the algorithm implementers use this interpolator as a baseline, but should perform a thorough validation.

3.6 Geolocation output parameter error computation

This section discusses how uncertainties in the geolocation inputs affect the expected geolocation accuracy. The input and output parameters in Table 3-3 are used and computed respectively for the reference photon *j*. For any reference photon there are three primary inputs that are essential for geolocation. These inputs are a product of the orbit and pointing determination of the instrument, and the timing of the photon round-trip measurement. They are shown below,

$$\left(\vec{X}_{ECI}, \hat{p}, \rho\right)$$

These inputs produce a geolocated bounce point location $\vec{B}_{ECI}$ in the inertial frame.

$$\vec{B}_{ECI} = \vec{X}_{ECI} + \rho \cdot \hat{p}$$

The term $\vec{X}_{ECI}$ is the inertial position of the transmit tracking point. The term $\hat{p}$ is the pointing vector transformed into the inertial frame and corrected for velocity aberration (rigorous formulation), and ρ is the transmit range corrected for instrument biases and path delay (Rigorous formulation: Section 2, Equation 2.3.10; Approximate Formulation: Section 3, Equation 3.1.2).

Geolocation errors are computed as the difference between the observed geolocation bounce point position computed with input errors ε, and the true bounce point position computed without input errors,

$$\Delta\vec{B}_{ECI} = \vec{B}_{ECI}^{\,observed} - \vec{B}_{ECI}^{\,truth}$$

The errors on the input parameters represent a perturbed state $x_0 + \Delta x$, that is perturbed by Δx from reference state x_0. A Taylor series expansion about this reference state yields,

$$\vec{B}_{ECI}(x_0 + \Delta x) = \vec{B}_{ECI}(x_0) + \left.\frac{\partial \vec{B}_{ECI}}{\partial x}\right|_{x_0} \Delta x + hot$$

Higher order terms hot are neglected in this study. The parameter x represents the inputs that are under study in this analysis. The geolocation errors can be rewritten in terms of the input parameters as,

$$\Delta\vec{B}_{ECI} = \vec{B}_{ECI}(x_0 + \Delta x) - \vec{B}_{ECI}(x_0), \qquad \Delta x = \varepsilon$$

The input errors are assumed to have zero-mean and be represented adequately by diagonal covariance matrix P,

$$\varepsilon \sim N(0, P), \qquad P = \begin{bmatrix} \sigma_x^2 & 0 & 0 \\ 0 & \sigma_y^2 & 0 \\ 0 & 0 & \sigma_z^2 \end{bmatrix}$$

The inertial geolocation errors can be transformed into the radial, in-track and cross-track (RIC) frame for an easier understanding of the error distribution,

$$\Delta\vec{B}_{RIC} = R_{ECI \to RIC} \Delta\vec{B}_{ECI}$$

- **Computing Radial, In-track and Cross-track Components (RIC)**

Given position $\vec{R}_{ECI}$ and velocity $\vec{V}_{ECI}$ vectors in a chosen reference frame (ECI) the transformation matrix from that chosen frame into radial, in-track and cross-track components can be expressed as,

$$\hat{z} = \frac{\vec{R}_{ECI}}{|\vec{R}_{ECI}|} = [z_1\ z_2\ z_3]$$

$$\hat{y} = \frac{\hat{z} \times \vec{V}_{ECI}}{|\hat{z} \times \vec{V}_{ECI}|} = [y_1\ y_2\ y_3]$$

$$\hat{x} = \frac{\hat{y} \times \hat{z}}{|\hat{y} \times \hat{z}|} = [x_1\ x_2\ x_3]$$

$$R_{ECI \to RIC} = \begin{bmatrix} z_1 & z_2 & z_3 \\ x_1 & x_2 & x_3 \\ y_1 & y_2 & y_3 \end{bmatrix}$$

$$\begin{bmatrix} u_{radial} \\ u_{intrack} \\ u_{cross} \end{bmatrix} = R_{ECI \to RIC} \begin{bmatrix} u_x \\ u_y \\ u_z \end{bmatrix}$$

where u is any vector expressed in the chosen frame in which the position and velocity vectors were provided. For the geolocation error analysis the inertial spacecraft position and velocity interpolated to the reference photon *j*'s bounce point time, $\vec{X}_{S/C}(t_B(j))$ and $\vec{V}_{S/C}(t_B(j))$ respectively are used to compute this reference frame.

- **Rigorous and Approximate Geolocation Algorithm Notes**

The rigorous and approximate geolocation algorithms were shown to agree to within tenths of a millimeter (Section 3, Equation 3.1.9) in total bounce point position during nominal reference ground track mapping and 5° scan maneuvers. In the following sections, we present the rigorous formulation to show how the exact relation between the geolocation inputs and outputs. In the end we present the relationships using the inputs from the approximate algorithm. Keep in mind that the approximate algorithm introduces additional error into the geolocation output, but that its magnitude is negligible and can be ignored. The most notable differences between the two algorithms are the approximation of the bounce point time and transmit range magnitude. The approximate algorithm uses the orbit position interpolated at the approximate bounce point time. Using the bounce point time accounts for velocity aberration and eliminates the need to use the spacecraft velocity to modify the pointing. The approximate algorithm also assumes that both transmit and receive ranges are equal in length. All of these simplifications produce nearly the same result as the rigorous formulation. Extensive testing was performed to validate the accuracy of the approximate algorithm and geolocation error output computations. We now present the theory of errors introduced into the geolocation output from uncertain input estimates. To see the direct implementation for the ICESat-2 mission, readers can skip ahead to Section 3.6.1, ICESat-2 implementation for reference photon *j*.

- **Position Errors**

Input errors on the instrument inertial position are given by,

$$\vec{X}_{ECI}^{\,observed} = \vec{X}_{ECI}^{\,truth} + \varepsilon, \qquad \Delta\vec{X}_{ECI} = \vec{X}_{ECI}^{\,observed} - \vec{X}_{ECI}^{\,truth} = \varepsilon$$

These errors have mean and variance statistics of,

$$E\{\varepsilon\} = 0, \qquad E\{\varepsilon_j \varepsilon_j^T\} = \sigma_j^2$$

We start with the geolocation computation,

$$\vec{B}_{ECI} = \vec{X}_{ECI} + \rho \cdot \hat{p}$$

We form the geolocation errors as,

$$\Delta\vec{B}_{ECI} = \vec{B}_{ECI}^{\,observed} - \vec{B}_{ECI}^{\,truth} = \upsilon$$

$$\Delta\vec{B}_{ECI} = \left(\vec{X}_{ECI}^{\,observed} + \rho \cdot \hat{p}\right) - \left(\vec{X}_{ECI}^{\,truth} + \rho \cdot \hat{p}\right) = \varepsilon$$

The resulting geolocation errors υ are simply equal to the position errors and have the exact error distribution,

$$E\{\upsilon\} = 0, \qquad E\left\{\upsilon_j \upsilon_j^T\right\} = \sigma_j^2$$

- **Velocity Errors**

Input errors on the instrument inertial velocity are given along with error statistics by,

$$\vec{V}_{ECI}^{\,observed} = \vec{V}_{ECI}^{\,truth} + \varepsilon, \qquad E\{\varepsilon\} = 0, \qquad E\left\{\varepsilon_j \varepsilon_j^T\right\} = \sigma_j^2$$

The velocity affects the inertial pointing vectors $\hat{u}$ when accounting for aberration. The pointing vector with aberration correction can be simplified as,

$$\hat{p} = \frac{c\hat{u} + \vec{V}_{ECI}^T}{\left|c\hat{u} + \vec{V}_{ECI}^T\right|}, \qquad \hat{p} \approx \frac{c\hat{u} + \vec{V}_{ECI}^T}{c}, \qquad c \gg \left|\vec{V}_{ECI}^T\right|$$

We start again with the geolocation computation,

$$\vec{B}_{ECI} = \vec{X}_{ECI} + \rho \cdot \hat{p}$$

We form the geolocation errors as,

$$\Delta\vec{B}_{ECI} = \vec{B}_{ECI}^{\,observed} - \vec{B}_{ECI}^{\,truth} = \upsilon$$

$$\Delta\vec{B}_{ECI} \approx \left(\vec{X}_{ECI} + \rho \cdot \frac{c\hat{u} + \vec{V}_{ECI}^T + \varepsilon}{c}\right) - \left(\vec{X}_{ECI} + \rho \cdot \frac{c\hat{u} + \vec{V}_{ECI}^T}{c}\right)$$

Simplifying,

$$\Delta\vec{B}_{ECI} \approx \rho \cdot \frac{\varepsilon}{c} = \Delta t\, \varepsilon$$

where $\Delta t = \frac{\rho}{c}$

The resulting geolocation errors υ are scaled with respect to the velocity errors by the Δt term.

$$E\{\upsilon\} \approx 0, \qquad E\left\{\upsilon_j \upsilon_j^T\right\} \approx \sigma_j^2 \Delta t^2$$

Velocity is not necessarily an input used in the approximate geolocation algorithm. The inertial position of the instrument tracking point used in the approximate solution is an interpolated position at the geolocated bounce point time. Velocity errors will manifest themselves as position errors if velocity is used in the interpolation or extrapolation computation. The elapsed time from transmit to the bounce point Δt is approximately 1.7 milli-seconds and given a conservative error

estimate of 5 m/sec would produce geolocation errors of less than 1 cm. Therefore, these errors are expected to be very small and can be neglected.

- **Ranging Errors**

Input errors on the 1-way transmit range leg are given by,

$$\rho^{observed} = \rho^{truth} + \varepsilon, \qquad E\{\varepsilon\} = 0, \qquad E\{\varepsilon\varepsilon^T\} = \sigma^2$$

We form the geolocation errors as,

$$\Delta\vec{B}_{ECI} = \vec{B}_{ECI}^{observed} - \vec{B}_{ECI}^{truth} = \upsilon$$

$$\Delta\vec{B}_{ECI} = \left(\vec{X}_{ECI} + \rho^{observed} \cdot \hat{p}\right) - \left(\vec{X}_{ECI} + \rho^{truth} \cdot \hat{p}\right)$$

$$\Delta\vec{B}_{ECI} = \varepsilon \cdot \hat{p}$$

The inertial pointing vector $\hat{p}$ provides the exact geolocation errors. If we assume the pointing is primarily along nadir the geolocation error expressed in the RIC frame simplify to,

$$E\{\upsilon\} \approx \begin{bmatrix}0\\0\\0\end{bmatrix}, \qquad E\{\upsilon_j\upsilon_j^T\} \approx \begin{bmatrix}\sigma^2\\0\\0\end{bmatrix}$$

- **Pointing Errors**

Let's define some useful quaternion notation first.

$$q = \begin{bmatrix}\varrho\\q_4\end{bmatrix}, \qquad \varrho = \begin{bmatrix}q_1\\q_2\\q_3\end{bmatrix} \equiv \sin\frac{\Delta\theta}{2}\begin{bmatrix}e_x\\e_y\\e_z\end{bmatrix}, \qquad q_4 \equiv \cos\frac{\Delta\theta}{2}$$

To transform from the observed or estimated state $q_{estimate}$ which is assumed to be close to the truth or true state q_{true}, one can define the rotation given by quaternion δq.

$$q_{true} = \delta q \otimes q_{estimate}$$

δq represents an error quaternion and is small. For small rotations,

$$\delta\varrho \approx \delta\alpha/2, \qquad \delta q_4 \approx 1$$

where $\delta\alpha$ has components of roll, pitch and yaw error angles $\begin{bmatrix}\phi\\\theta\\\psi\end{bmatrix}$ for any rotation sequence. Attitude or pointing errors are expressed as rotation angles from the δq error quaternion.

$$\begin{bmatrix}\phi\\\theta\\\psi\end{bmatrix} \approx 2\begin{bmatrix}\delta q_1\\\delta q_2\\\delta q_3\end{bmatrix}$$

These errors express the uncertainty in the orientation of a desired frame (LF for ICESat-2 application) and impacts the accuracy of the inertial pointing unit vector $\hat{\rho}$. A laser-pointing vector in the inertial frame (ECI) is transformed into a pointing vector in the LF frame, where the errors are expressed.

$$\hat{L}_{LF} = R^{T}_{LF \to ECI} \hat{L}_{ECI}$$

The pointing vector estimate, $\hat{L}^{estimate}_{LF}$ is computed using the true or known pointing vector, and applying roll, pitch and yaw error angle rotations,

$$\hat{L}^{estimate}_{LF} = R^{T}_{\phi} R^{T}_{\theta} R^{T}_{\psi} \hat{L}^{true}_{LF}$$

The rotation matrices above are transposed (*T* denotes the transpose of the rotation matrix) because the attitude errors take us from the estimated state to the true state,

$$\hat{L}^{true}_{LF} = R_{\psi} R_{\theta} R_{\phi} \hat{L}^{estimate}_{LF}$$

The rotation matrices are a function of the Euler roll, pitch and yaw error angles,

$$R_{\phi} = \begin{bmatrix} 1 & 0 & 0 \\ 0 & \cos\phi & \sin\phi \\ 0 & -\sin\phi & \cos\phi \end{bmatrix}, \qquad R_{\theta} = \begin{bmatrix} \cos\theta & 0 & -\sin\theta \\ 0 & 1 & 0 \\ \sin\theta & 0 & \cos\theta \end{bmatrix},$$

$$R_{\psi} = \begin{bmatrix} \cos\psi & \sin\psi & 0 \\ -\sin\psi & \cos\psi & 0 \\ 0 & 0 & 1 \end{bmatrix}$$

Finally, the pointing is expressed in the inertial frame,

$$\hat{\rho} = R_{LF \to ECI} \hat{L}^{estimate}_{LF}$$

where it is used to compute the representative geolocation errors.

Using the known or true laser pointing unit vector of interest in the LF frame $\hat{L}^{true}_{LF}$, the errors are given as,

$$\Delta\vec{B}_{ECI} = \vec{B}^{\,observed}_{ECI} - \vec{B}^{\,truth}_{ECI} = \upsilon$$

$$\Delta\vec{B}_{ECI} = \left(\vec{X}_{ECI} + \rho \cdot \hat{p}^{observed}\right) - \left(\vec{X}_{ECI} + \rho \cdot \hat{p}^{truth}\right)$$

Expressed in the LF frame,

$$\Delta\vec{B}_{LF} = \rho\left(\hat{L}^{estimate}_{LF} - R_{\psi} R_{\theta} R_{\phi} \hat{L}^{estimate}_{LF}\right) = \rho\left(I - R_{\psi} R_{\theta} R_{\phi}\right)\hat{L}^{estimate}_{LF}$$

And in the inertial frame,

$$\Delta\vec{B}_{ECI} = \rho R_{LF \to ECI}\left(\hat{L}^{estimate}_{LF} - R_{\psi} R_{\theta} R_{\phi} \hat{L}^{estimate}_{LF}\right) = \rho R_{LF \to ECI}\left(I - R_{\psi} R_{\theta} R_{\phi}\right)\hat{L}^{estimate}_{LF}$$

If the laser frame axes are aligned or near the spacecraft body axes, a simple and generally accurate approach is to assume pointing near nadir, then the geolocation errors $\Delta\vec{B}_{LF}$ are approximately,

$$\Delta\vec{B}_{LF} \approx \rho \begin{bmatrix} \tan\theta \\ -\tan\phi \\ 0 \end{bmatrix}$$

where and θ and ϕ are the pitch and roll error angles respectively. Yaw error angles introduce little to no error for nadir pointing beams. The geolocation errors can then be transformed into any frame of interest.

To summarize, the attitude or pointing errors are provided as small rotation angles computed form the δq error quaternion with statistical distributions given by,

$$\begin{bmatrix} \phi \\ \theta \\ \psi \end{bmatrix} \approx 2 \begin{bmatrix} \delta q_1 \\ \delta q_2 \\ \delta q_3 \end{bmatrix} = \varepsilon, \qquad E\{\varepsilon\} = \begin{bmatrix} 0 \\ 0 \\ 0 \end{bmatrix}, \qquad E\{\varepsilon\varepsilon^T\} = \begin{bmatrix} \sigma_\phi^2 & 0 & 0 \\ 0 & \sigma_\theta^2 & 0 \\ 0 & 0 & \sigma_\psi^2 \end{bmatrix}$$

If the laser frame is closely aligned to the spacecraft body frame axes, and assuming nadir pointing and small rotations we arrive at,

$$\Delta\vec{B}_{LF} \approx \rho \begin{bmatrix} \tan\theta \\ -\tan\phi \\ 0 \end{bmatrix} \approx \rho \begin{bmatrix} \theta \\ -\phi \\ 0 \end{bmatrix}, \text{for small rotations}$$

$$E\{\Delta\vec{B}_{LF}\} \approx \begin{bmatrix} 0 \\ 0 \\ 0 \end{bmatrix}, \qquad E\{\Delta\vec{B}_{LF}\Delta\vec{B}_{LF}^T\} \approx \rho^2 \begin{bmatrix} \sigma_\theta^2 & 0 & 0 \\ 0 & \sigma_\phi^2 & 0 \\ 0 & 0 & 0 \end{bmatrix}$$

Or for an exact representation:

$$\Delta\vec{B}_{LF} = \rho\left(I - R_\psi R_\theta R_\phi\right)\hat{L}_{LF}^{true}$$

Where the statistical mean $E\{\Delta\vec{B}_{LF}\}$, and covariance matrix $E\{\Delta\vec{B}_{LF}\Delta\vec{B}_{LF}^T\}$ are given in the following section for inertial geolocation errors.

- **Timing Errors**

Errors associated with the time tags of each input realize themselves as errors in the inputs themselves. For each input the partial derivative with respect to a change in time ∂t can be computed,

$$\left(\vec{X}_{ECI}, \hat{p}, \rho\right) \rightarrow \left(\frac{\partial\vec{X}_{ECI}}{\partial t}, \frac{\partial\hat{p}}{\partial t}, \frac{\partial\rho}{\partial t}\right)$$

The geolocation computation in the inertial frame:

$$\vec{B}_{ECI} = \vec{X}_{ECI} + \rho \cdot \hat{p}$$

Produces a change in geolocated bounce point location $\Delta\vec{B}_{ECI}$ due to an error in reported time tag dt,

$$\Delta\vec{B}_{ECI} = \frac{\partial \vec{X}_{ECI}}{\partial t} dt + \frac{\partial \rho}{\partial t} dt \cdot \hat{p} + \rho \cdot \frac{\partial \hat{p}}{\partial t} dt$$

It is a requirement for ICESat-2 to have time tags corrected to within 100 nsec of GPS time. Given a spacecraft velocity of 7600 m/sec, this would produce sub-mm geolocation errors. Attitude is practically constant over these time scales and would not introduce measurable differences from errors in pointing. Range errors are expected to include errors from inexact timing of the photon round-trip observation and are different from the time tag errors introduced in this section. Therefore, time tags errors are ignored in ATL03G.

3.6.1 ICESat-2 implementation for reference photon *j*

The inertial geolocation error estimate, $\Delta\vec{B}_{ECI}$ was derived in the preceding theoretical section. Now we wish to compute the statistical covariance of these errors. This section uses the exact notation from Section 3's approximate algorithm formulation to compute the inertial geolocation error covariance estimate, $cov\left(\Delta\vec{B}_{ECI}^{total}\right)$ for reference photon *j*. The procedure (steps 1-4) discussed in the following section, Error *Outputs for ATL03G (Section 3.6.2)* are then followed to produce the output parameters of Table 3-3.

The input errors are assumed to represent a Gaussian distribution with no mean value or biases. Other simplifications to the error estimation process include neglecting velocity and time tag errors due to their minimal impact on the geolocation output. Error input and output estimates are also reported giving only the square root of the diagonal elements of the covariance matrix. This means that if there were to exist any strong cross-correlations between the inputs errors we could misrepresent the computed error output statistics.

Again, the input errors are assumed to be zero-mean and be represented by the diagonal covariance matrix *P* of general form,

$$\varepsilon \sim N(0, P), \qquad P = \begin{bmatrix} \sigma_1^2 & 0 & 0 \\ 0 & \ddots & 0 \\ 0 & 0 & \sigma_N^2 \end{bmatrix}$$

where the uncertainty estimates σ_i are given for elements $i = 1{:}N$. The uncertainty estimates must be interpolated to either the reference photon's transmit or bounce point time, $t_T(j)$ and $t_B(j)$ respectively to accurately compute a geolocation error covariance estimate.

The components of the inertial pointing vector found in Equation 3.1.7 are used often in the following section and are expressed as,

$$\begin{bmatrix} u_x \\ u_y \\ u_z \end{bmatrix} = \hat{L}_{ECI}\left(t_T(j)\right) = \hat{p}(j)$$

And finally, the transmit range ignoring atmospheric path delay corrections is also used and approximated in Equation 3.1.2 as,

$$\rho = \frac{tof(j)}{2} * c \quad - \quad \rho_{bias}\left(t_T(j)\right)$$

Now we can compute the geolocation error covariance estimate for each error input and compute a total error estimate.

- **Step 1: Position**

Orbit error uncertainty time histories, $\delta\vec{X}^{\sigma}_{S/C}$ in the RIC frame are provided in ANC04 and correspond directly to the provided spacecraft positions.

$$\delta\vec{X}^{\sigma}_{S/C}(t_T(j)) = \begin{bmatrix}\sigma_x \\ \sigma_y \\ \sigma_z\end{bmatrix}$$

$$cov\left(\Delta\vec{B}^{orbit}_{RIC}\right) = \begin{bmatrix}\sigma_x^2 & 0 & 0 \\ 0 & \sigma_y^2 & 0 \\ 0 & 0 & \sigma_z^2\end{bmatrix}$$

$$cov\left(\Delta\vec{B}^{orbit}_{ECI}\right) = R^T_{ECI\rightarrow RIC}(t_T(j))cov\left(\Delta\vec{B}^{orbit}_{RIC}\right)R_{ECI\rightarrow RIC}$$

- **Step 2: Ranging**

Ranging error uncertainty time histories, $\delta\rho^{\sigma}$ are provided in ANC04 which includes the total uncertainty in 1-way ranging due to the time-of-flight measurement, bias estimate, and atmospheric path delay.

$$\sigma_{ranging} = \delta\rho^{\sigma}$$

$$cov\left(\Delta\vec{B}^{ranging}_{ECI}\right) = \begin{bmatrix}\left(\sigma_{ranging}u_x\right)^2 & u_xu_y\sigma^2_{ranging} & u_xu_z\sigma^2_{ranging} \\ u_xu_y\sigma^2_{ranging} & \left(\sigma_{ranging}u_y\right)^2 & u_yu_z\sigma^2_{ranging} \\ u_xu_z\sigma^2_{ranging} & u_yu_z\sigma^2_{ranging} & \left(\sigma_{ranging}u_z\right)^2\end{bmatrix}$$

- **Step 3: Pointing**

Pointing error uncertainty time histories, $\delta\alpha^{\sigma}$ are provided in ANC05 and correspond to the uncertainty in the pointing vector estimates expressed in the laser frame $\hat{L}_{LF}$.

$$\delta\alpha^{\sigma}(t_T(j)) = \begin{bmatrix}\sigma_{\phi_{LF}} \\ \sigma_{\theta_{LF}} \\ \sigma_{\psi_{LF}}\end{bmatrix}$$

The statistical covariance of these errors in the laser frame are,

$$cov\left(\begin{bmatrix}\phi_{LF}\\ \theta_{LF}\\ \psi_{LF}\end{bmatrix}\right) = E\left\{\begin{bmatrix}\phi_{LF}\\ \theta_{LF}\\ \psi_{LF}\end{bmatrix}\begin{bmatrix}\phi_{LF}\\ \theta_{LF}\\ \psi_{LF}\end{bmatrix}^T\right\} = \begin{bmatrix}\sigma^2_{\phi_{LF}} & 0 & 0\\ 0 & \sigma^2_{\theta_{LF}} & 0\\ 0 & 0 & \sigma^2_{\psi_{LF}}\end{bmatrix}$$

These errors need to be expressed in the inertial frame to estimate the geolocation errors,

$$cov\left(\begin{bmatrix}\phi\\ \theta\\ \psi\end{bmatrix}\right) = R_{LF\rightarrow ECI}(t_T(j))cov\left(\begin{bmatrix}\phi_{LF}\\ \theta_{LF}\\ \psi_{LF}\end{bmatrix}\right)R^T_{LF\rightarrow ECI}(t_T(j))$$

$$cov\left(\begin{bmatrix}\phi\\ \theta\\ \psi\end{bmatrix}\right) = \begin{bmatrix}\sigma^2_{\phi} & corr_{\phi\theta} & corr_{\phi\psi}\\ corr_{\phi\theta} & \sigma^2_{\theta} & corr_{\theta\psi}\\ corr_{\phi\psi} & corr_{\theta\psi} & \sigma^2_{\psi}\end{bmatrix}$$

The inertial geolocation errors,

$$\Delta\vec{B}^{pointing}_{ECI}(j) = \rho\left(I - R_{\psi}R_{\theta}R_{\phi}\right)\hat{L}_{ECI}\left(t_T(j)\right)$$

Can be simplified using small angle approximations,

$$R_{\psi}R_{\theta}R_{\phi} \approx \begin{bmatrix}1 & \psi & -\theta\\ -\psi & 1 & \phi\\ \theta & -\phi & 1\end{bmatrix}$$

To produce the final result,

$$\Delta\vec{B}^{pointing}_{ECI}(j) \approx \rho\begin{bmatrix}\theta u_z - \psi u_y\\ \psi u_x - \phi u_z\\ \phi u_y - \theta u_x\end{bmatrix}$$

The covariance of the geolocation errors from pointing errors are given as,

$$cov\left(\Delta\vec{B}^{pointing}_{ECI}\right) = \rho^2\begin{bmatrix}(\sigma_\theta u_z)^2 + \left(\sigma_\psi u_y\right)^2 - 2u_y u_z corr_{\theta\psi} & corr^{pointing}_{xy} & corr^{pointing}_{xz}\\ corr^{pointing}_{xy} & \left(\sigma_\psi u_x\right)^2 + \left(\sigma_\phi u_z\right)^2 - 2u_x u_z corr_{\phi\psi} & corr^{pointing}_{yz}\\ corr^{pointing}_{xz} & corr^{pointing}_{yz} & \left(\sigma_\phi u_y\right)^2 + (\sigma_\theta u_x)^2 - 2u_x u_y corr_{\phi\theta}\end{bmatrix}$$

With off-diagonal terms given,

$$corr^{pointing}_{xy} = \left[corr_{\theta\psi}u_x u_z - corr_{\phi\theta}u_z u_z - \sigma^2_{\psi}u_x u_y + corr_{\phi\psi}u_y u_z\right]$$

$$corr^{pointing}_{yz} = \left[corr_{\phi\psi}u_x u_y - corr_{\theta\psi}u_x u_x - \sigma^2_{\phi}u_y u_z + corr_{\phi\theta}u_x u_z\right]$$

$$corr^{pointing}_{xz} = \left[corr_{\phi\theta}u_y u_z - corr_{\phi\psi}u_y u_y - \sigma^2_{\theta}u_x u_z + corr_{\theta\psi}u_x u_y\right]$$

- **Step 4: Total geolocation error estimate:**

All the individual error covariance estimates can be combined together to produce a total error covariance estimate for reference photon *j* $cov\left(\Delta\vec{B}_{ECI}^{total}\right)$,

$$cov\left(\Delta\vec{B}_{ECI}^{total}\right) = cov\left(\Delta\vec{B}_{ECI}^{orbit}\right) + cov\left(\Delta\vec{B}_{ECI}^{ranging}\right) + cov\left(\Delta\vec{B}_{ECI}^{pointing}\right)$$

Now the inertial error covariance estimate, $cov\left(\Delta\vec{B}_{ECI}^{total}\right)$ can be transformed into geodetic, along and cross track coordinates as shown in the next section.

- **Height scaling factor**

It is desired that the group of photons, $i = 1 \rightarrow N$ photons given in Equation 3.1.1 are selected over short time scales such that the errors associated with the reference photon are representative of the errors for all other photons in that group. It is assumed that orbit and pointing errors over this time span are generally constant, which would provide consistent errors across the group. For photons that noticeably differ in height from the reference photon the geolocation errors begin to deviate from the errors of the reference photon. A scaling factor can be used to compute error estimates for all photons in the group. Orbit and ranging uncertainties affect every photon in the same way. However, photons can have range observations that vary significantly in the group. Therefore, each photon 1-way range accurately scales the errors of the reference photon in the group. The pointing error covariance estimate is revisited again to scale the errors.

The partial with respect to a change in measured range is given as,

$$\frac{\partial cov\left(\Delta\vec{B}_{ECI}^{pointing}\right)}{\partial\rho} = 2\rho\begin{bmatrix}(\sigma_\theta u_z)^2 + \left(\sigma_\psi u_y\right)^2 - 2u_y u_z corr_{\theta\psi} & corr_{xy}^{pointing} & corr_{xz}^{pointing} \\ corr_{xy}^{pointing} & \left(\sigma_\psi u_x\right)^2 + \left(\sigma_\phi u_z\right)^2 - 2u_x u_z corr_{\phi\psi} & corr_{yz}^{pointing} \\ corr_{xz}^{pointing} & corr_{yz}^{pointing} & \left(\sigma_\phi u_y\right)^2 + (\sigma_\theta u_x)^2 - 2u_x u_y corr_{\phi\theta}\end{bmatrix}$$

The output height scale factor is then:

$$h_{scale} = \frac{\partial cov\left(\Delta\vec{B}_{ECI}^{pointing}\right)}{\partial\rho}$$

And a new error covariance estimate for the *i*th photon is simply,

$$cov\left(\Delta\vec{B}_{ECI}^{total}\right)(i) = cov\left(\Delta\vec{B}_{ECI}^{total}\right)(j) + h_{scale}(\rho(i) - \rho(j))$$

The procedure introduced in the next section is then followed to transform the new errors into different components (geodetic and along/cross-track). It is important to note that this computation scales all components, not just height. Because pointing is primarily along nadir, the horizontal changes could be ignored.

A study of the photon geolocation error estimates within a group of photons with different transmit ranges suggests that the height scaling factor could be ignored if the photons in a group are within kilometers of each other. A photon 1 kilometer away in transmit range from the reference photon has error estimates within 1 centimeter of the reference photon's error estimates for radial, in-track and cross-track components at 5 degree off-pointing (see Section 3.6.2 Summary).

3.6.2 Error Outputs for ATL03G

Input errors for the geolocation error analysis are provided in the ancillary input files. Table 3-3 shows the input error variables provided with 1σ uncertainty. The errors are transformed into corresponding 1σ geolocation error estimates that are also listed in Table 3-3.

The geolocation computation is done in an inertial frame, but the output uncertainty parameters are given in different reference frame coordinates. To get the outputs in geodetic coordinates it is necessary to transform the inertial geolocation position errors into ECF coordinates (as in Section 3.1, STEP 6), and then into ENU coordinates as in Section 3.3. Finally, the ENU coordinates are transformed into delta latitude $\Delta\phi$, delta longitude $\Delta\lambda$, and delta ellipsoid height Δh, as presented in Section 3.4.

Below, the procedure is given once the inertial geolocation error covariance estimate $cov\left(\Delta\vec{B}_{ECI}^{total}\right)$ is computed for reference photon j:

Step 1: Transform $cov\left(\Delta\vec{B}_{ECI}^{total}\right)$ inertial geolocation error covariance estimate into the ECF frame, $cov\left(\Delta\vec{B}_{ECF}^{total}\right)$. See Section 3.1, STEP 6 for more details.

$$cov\left(\Delta\vec{B}_{ECF}^{total}\right) = R_{ECI\rightarrow ECF}\left(t_B(j)\right)\, cov\left(\Delta\vec{B}_{ECI}^{total}\right) R_{ECI\rightarrow ECF}^{T}\left(t_B(j)\right)$$

Step 2: Transform $cov\left(\Delta\vec{B}_{ECF}^{total}\right)$ ECF geolocation error covariance estimate into the ENU frame. See section 3.3 for more details.

$$R_{ECF\rightarrow ENU} = \begin{bmatrix} -sin\lambda & cos\lambda & 0 \\ -cos\lambda sin\phi & -sin\lambda sin\phi & cos\phi \\ cos\lambda cos\phi & sin\lambda cos\phi & sin\phi \end{bmatrix}$$

ϕ and λ are the geodetic latitude and longitude (Section 3.2) of the reference photon bounce point position.

$$cov\left(\Delta\vec{B}_{ENU}^{total}\right) = R_{ECF\rightarrow ENU}\, cov\left(\Delta\vec{B}_{ECF}^{total}\right) R_{ECF\rightarrow ENU}^{T}$$

$$cov\left(\Delta\vec{B}_{ENU}^{total}\right) = \begin{bmatrix} \sigma_E^2 & \sigma_{EN} & \sigma_{EU} \\ \sigma_{EN} & \sigma_N^2 & \sigma_{NU} \\ \sigma_{EU} & \sigma_{NU} & \sigma_U^2 \end{bmatrix}$$

Step 3: Transform $cov\left(\Delta\vec{B}_{ENU}^{total}\right)$ ENU geolocation error covariance estimate into geodetic coordinates. The geodetic output errors in Table 3-3 are given,

$$\Delta\phi(j) = \frac{\sigma_N}{R_E}, \quad \Delta\lambda(j) = \frac{\sigma_E}{R_E \cos\phi}$$

$$\Delta h(j) = \sigma_U$$

Where geodetic latitude and longitude errors, $\Delta\phi$ and $\Delta\lambda$ are converted into degrees. See Section 3.4 for more details.

Step 4: Transform $cov\left(\Delta\vec{B}_{ECI}^{total}\right)$ inertial geolocation error covariance estimate into RIC components. To get corresponding in-track and cross-track (*sigma_along* and *sigma_across*) error components in Table 3-3,

$$cov\left(\Delta\vec{B}_{RIC}^{total}\right) = R_{ECI\to RIC}\, cov\left(\Delta\vec{B}_{ECI}^{total}\right) R_{ECI\to RIC}^{T}$$

$$cov\left(\Delta\vec{B}_{ECI}^{total}\right) = \begin{bmatrix} \sigma_R^2 & \sigma_{RI} & \sigma_{RC} \\ \sigma_{RI} & \sigma_I^2 & \sigma_{IC} \\ \sigma_{RC} & \sigma_{IC} & \sigma_C^2 \end{bmatrix}$$

$$sigma_{along} = \sigma_I, \quad sigma\_across = \sigma_C$$

See paragraph *Computing Radial, In-track and Cross-track Components (RIC)* under Section 3.6 for more details on the ECI to RIC transformation.

- **Summary**

A simulation with position, velocity, ranging and attitude error input histories was performed to compare predicted and computed geolocation errors. Geolocation errors were computed from the difference between true bounce point positions and estimated bounce points with the input errors. The true bounce point position came from using error free inputs and computing bounce points on the WGS-84 reference ellipsoid. The estimated bounce point came from using the true round-trip range observations and adding in errors to all the inputs including the range observations themselves. Both the rigorous and approximate algorithms themselves were tested to observe the error results. Predicted geolocation error estimates used the error histories on the inputs to analytically calculate a history of geolocation errors. The equations presented in this section were used to predict these errors. The figure below shows the numerically computed and analytically predicted geolocation errors in the RIC frame. The predicted errors lay on top of the numerically computed (truth) errors.

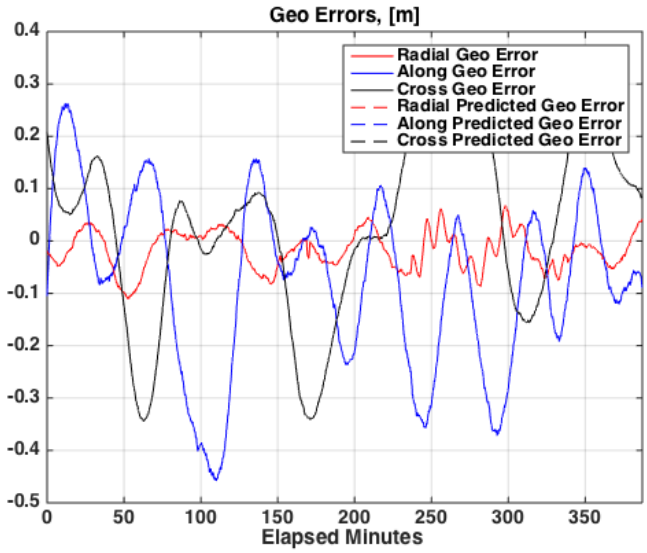

Figure 3-1 Simulated (computed) errors versus predicted geolocation errors

The next figure differences the predicted and computed errors from using the rigorous algorithm. The difference is many orders of magnitude below the geolocation errors themselves.

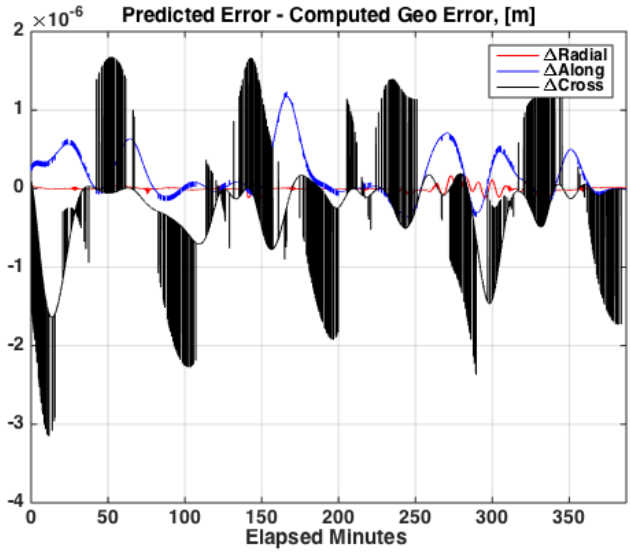

Figure 3-2 Difference between predicted and computed errors using rigorous geolocation

The next figure differences the predicted and computed errors from using the approximate algorithm. The difference is many orders of magnitude below the geolocation errors themselves. Notice that the radial prediction is about 0.016 cm off from the computed error. This is an artifact of using the approximate algorithm to perform the geolocation. The error is negligible.

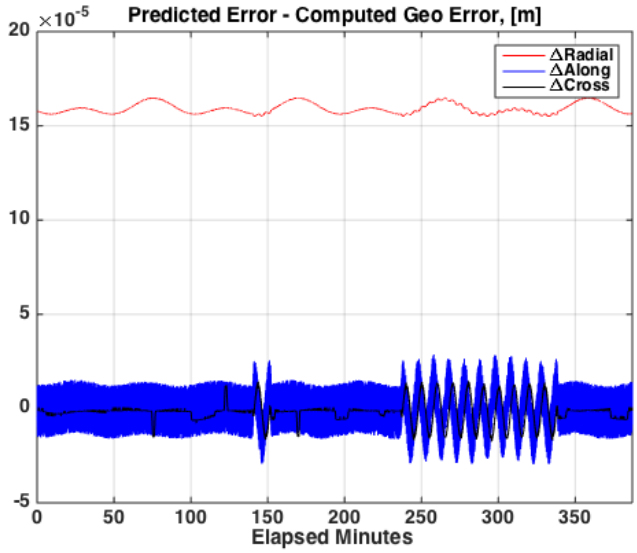

Figure 3-3 Difference between predicted and computed errors using approximate geolocation

The covariance matrix is shown for both the rigorous and approximate algorithms below. The predictions are very close to the computed error in both cases. The predictions do not vary because the formulas presented in this section do not change. The values used for bounce time, transmit range and other parameters are the approximated ones used in Section 3.1.

Table 3-4 Rigorous algorithm and predicted geolocation error covariance matrix [cm^2]

Radial	Intrack	Cross
13.025	-17.251	5.587
-17.251	275.207	-60.028
5.587	-60.028	294.858

Table 3-5 Approximate algorithm geolocation error covariance matrix [cm^2]

Radial	Intrack	Cross

13.026	-17.249	5.586
-17.249	275.208	-60.027
5.586	-60.027	294.858

Below, the approximate algorithm (with no input errors) differences with respect to the true bounce point are shown. Notice the 0.016 cm radial difference that appears in Figure 3-3 above.

Table 3-6 Approximate algorithm error statistics [cm]

	Mean	1σ
Radial	-0.016	0.000
Intrack	0.000	0.001
Cross	0.000	0.001

Extensive testing through simulation has verified that the equations presented in this section produce accurate error estimates to sub-millimeter precision.

Finally, some nominal error estimates (meters) are presented in Table 3-4 on the expected uncertainty in geolocation estimation for a typical satellite configuration with given error inputs and orbit information listed below:

- POD RIC: {3 10 10} cm
- TOF Ranging: 2 cm
- PPD Laser Frame: {10 10 30} μrad
- Altitude: 489 km

Table 3-7 Nominal Geolocation Error Estimates, 1σ (meters)

Off-pointing [deg]	0	1	1.7	5
σ_{Radial}	0.036	0.093	0.151	0.433
$\sigma_{Intrack}$	4.935	4.936	4.937	4.955

σ_{Cross}	4.931	4.931	4.931	4.932

The error estimates increase gradually when pointing further from nadir. The 1.7 degree off-point approximately corresponds to the expected maximum pointing to a vegetation track during the mission, and 5 degrees represents the off-pointing limit for science collection.

3.7 Time Systems

The integration of the satellite equations of motion requires a uniform time system. The system used in the POD processing software, GEODYN, is the Terrestrial Dynamic Time (TDT) (also referred to as Terrestrial Time (TT)) [*Guinot, 1991, McCarthy, 1996*]. The TDT time is in practice determined from the International Atomic Time (TAI):

$$TDT = TAI + 32.184 \text{ s}$$

The TDT time must be converted to the conventional time scales used by most observers for time-tagging satellite observations and tracking data. The conventional time scales relevant to most laser altimeter missions are UTC and GPS time.

UTC, or Coordinated Universal Time, is an atomic time system which runs at the same rate as TAI, but is periodically adjusted by one second steps in order to keep it near the UT1 time system. The UT1 time system is the non-uniform time determined by observations of the stars from the non-uniformly rotating Earth, after correcting for polar motion. Correction factors relating UTC and UT1, and UTC and TAI, are provided by the IERS Bulletin B or by the USNO Rapid Service (IERS Bulletin A).

GPS Time [*Hofmann-Wellenhof et al., 1994*] is the time system to which all GPS clocks and observables are referenced. It is also an atomic time system derived from TAI. GPS Time can be computed from:

$$GPS = TAI - 19.000 \text{ s}$$

Calendar dates are referenced to the Julian Date (JD) or the Modified Julian Date (MJD) [*Taff, 1985*]. The current standard epoch is J2000.0 which is JD = 2451545.0, or January 1.5, 2000.

The GPS system uses the GPS standard epoch of JD = 2444244.5 or January 6.0, 1980. An important unit for the GPS system is the GPS week, which is defined as:

$$\text{GPS week} = \text{INT}\,[(JD - 2444244.5) / 7]$$

where INT[x] is the largest integer smaller than x.

3.8 Reference Frames

The current ECI frame employed for the ICESat-2 altimeter measurement modeling and geolocation is the geocentric realization of the International Celestial Reference System (ICRS), namely the ICRF Geocentric mean equator and equinox of 2000 Jan 1.5 (J2000.0) defined by the International Earth Rotation Service (IERS), and realized by use of the JPL Development Ephemeris DE403, and the Lunar Ephemeris LE403 [Standish et al., 1995 & *Petit and Luzum, 2010*].

The geodetic reference frame, which is consistently used in the analysis of altimeter data, is the International Terrestrial Reference Frame (ITRF). The ITRF definition and other current modeling recommendations of the IERS are documented in the "IERS Conventions" [*Petit and Luzum, 2010*].

Transformation between the ICRF and the ITRF is accomplished using the following equation:

$$\left[ICRF\right] = P(t)N(t)R(t)W(t)\left[ITRF\right]$$

where

P(t) = precession transformation
N(t) = nutation transformation
R(t) = transformation due to rotation of the Earth
W(t) = polar motion transformation

The precession – nutation transformations follows IAU 2000 [*Cappola et al., 2009*]. The rotation transformation is just a rotation around the Earth's spin axis by $-\theta_g$, where θ_g is the Greenwich True Sidereal Time at epoch t. The *R(t)* and *W(t)* transformations are described in [*Petit and Luzum, 2010*].

3.9 Time varying surface displacement models

The models, algorithms and constants used in computing the time varying surface displacement effects are documented in the ATL03 Section 6.0 ATBD.

3.10 Geophysical constants and standards.

Geophysical constants and standards are documented in the POD and Instrument Parameter Calibration ATBD and are congruent with ATL03 Section 6.0.

3.11 Test data and Validation

The GSFC POD & Calibration team has a full simulation capability including orbits, attitude, pointing, and altimeter ranging to modeled surfaces. This simulation capability has been used for many aspects of the project including simulating data for the ATLAS on-board algorithm development and performance analysis.

A 14-day Orbit in the Life simulation has been created including repeat/vegetation transitions, ocean scans, and targets of opportunity. As part of this simulation, altimeter ranges to the WGS-84 reference ellipsoid are simulated at 1 and 10 Hz. A single perfect photon observation and transmit time tag are computed at these rates. This data set will form the "truth" data. The data inputs noted in Table 3-1 will be created from this simulation and the output data defined in Tables 3-2 and 3-3 will be created for the full 14-day simulation. The simulated input test data from the 14-day simulation will be used by the SIPS to compute the geolocation output data noted in Table 3-2. These SIPS computed data will then be compared to the POD & Calibration team's Table 3-2 data computed from the simulated Table 3-1 data.

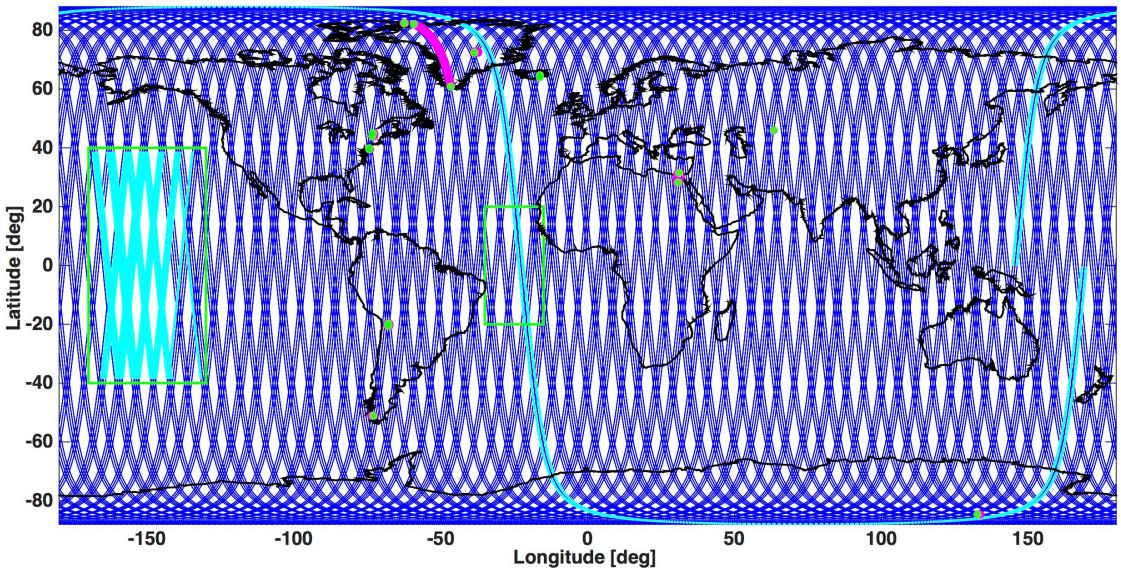

Figure 3-4 Instrument Calibration and Target of Opportunity Map

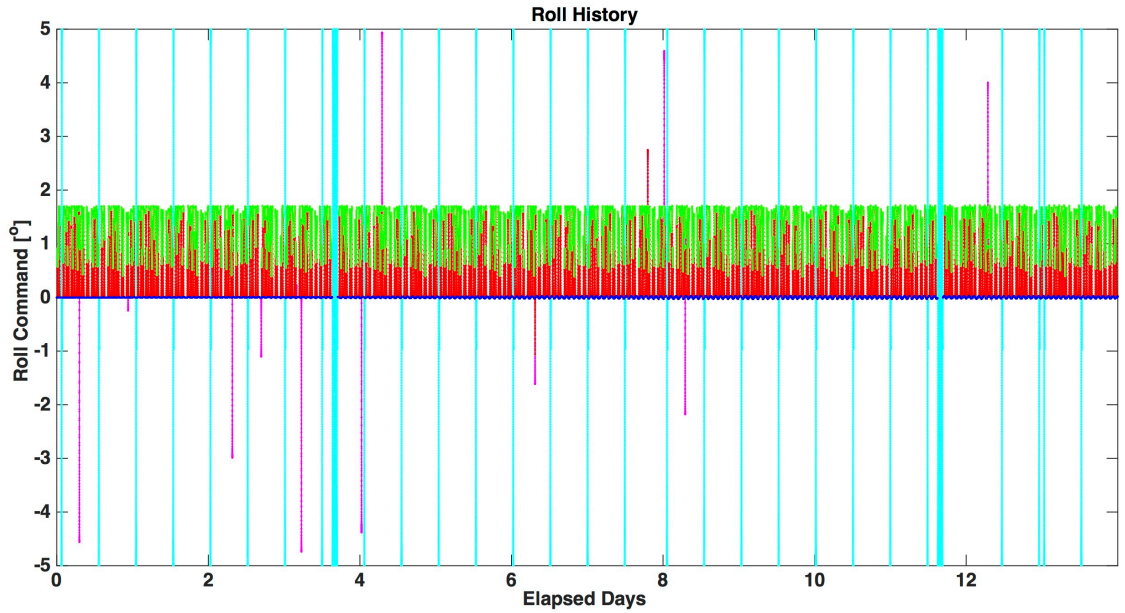

Figure 3-5 Spacecraft Attitude History for Roll Axis

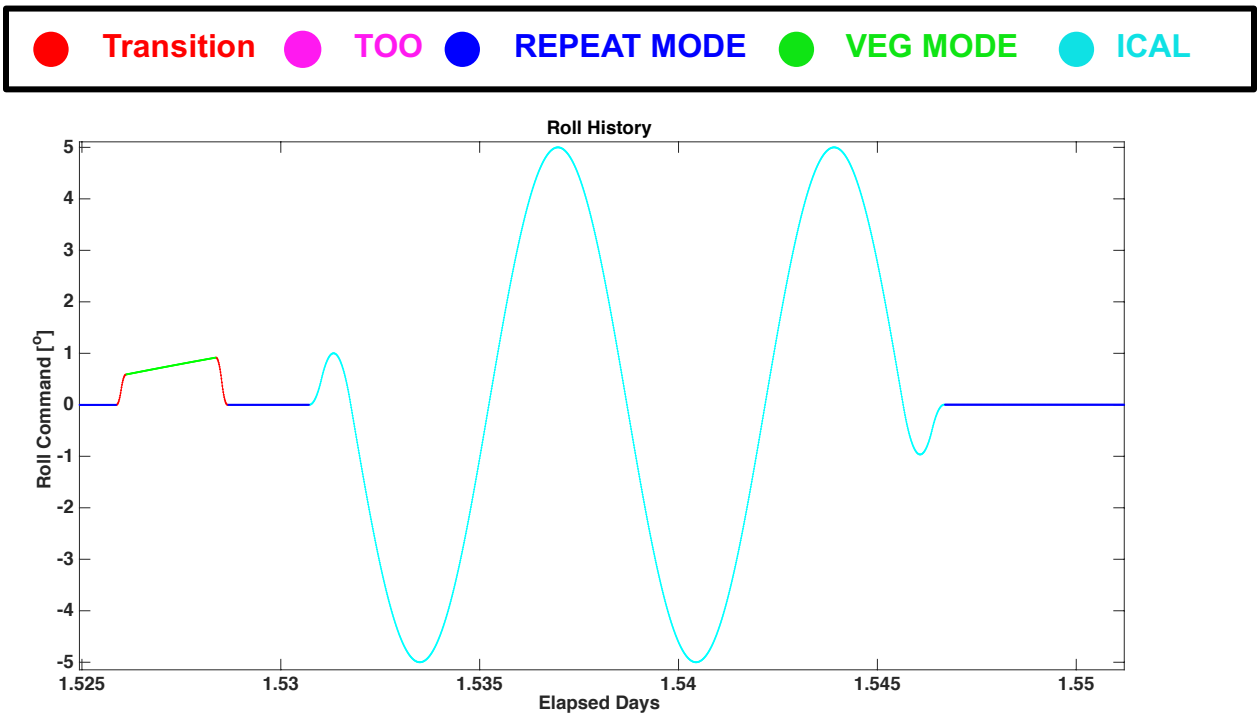

Figure 3-6 Instrument Calibration Scan Attitude History

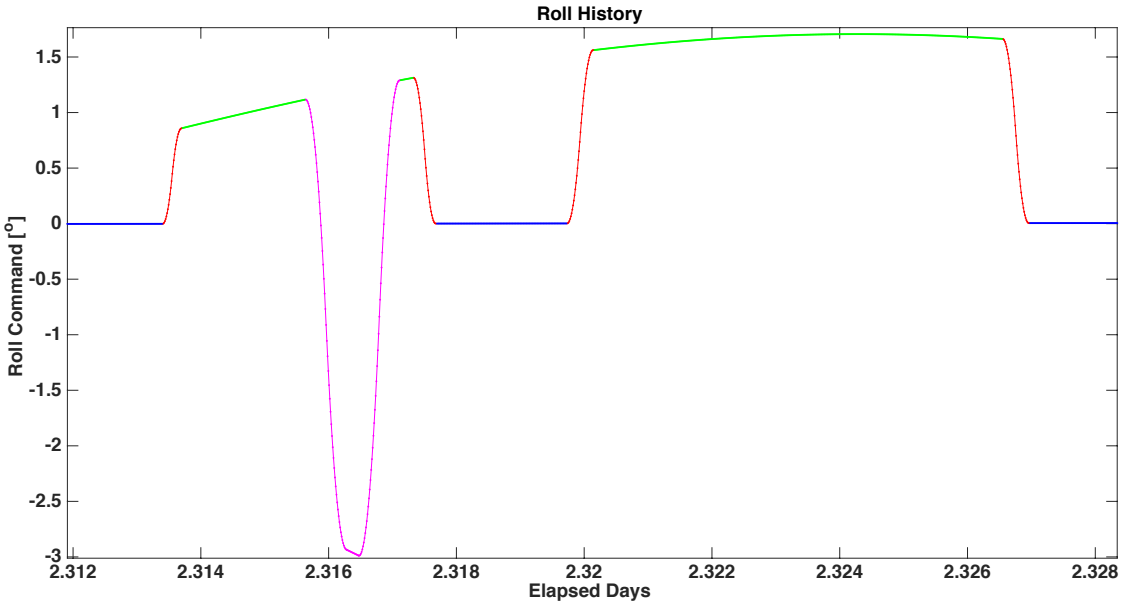

Figure 3-7 Target of Opportunity Attitude History

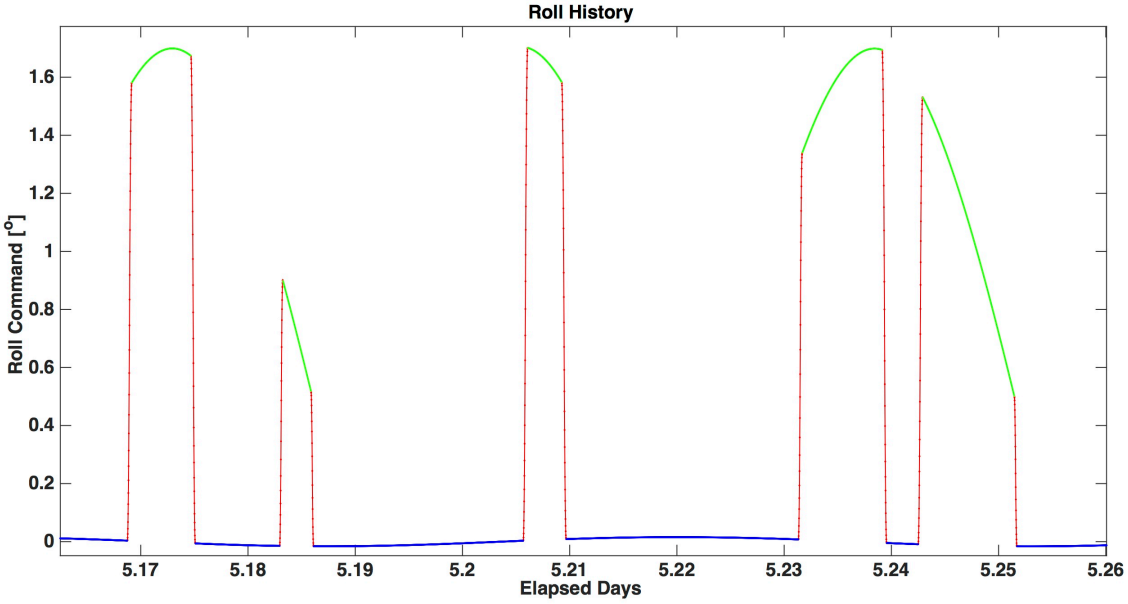

Figure 3-8 Reference Ground-Track Pointing and Vegetation Off-pointing Attitude History

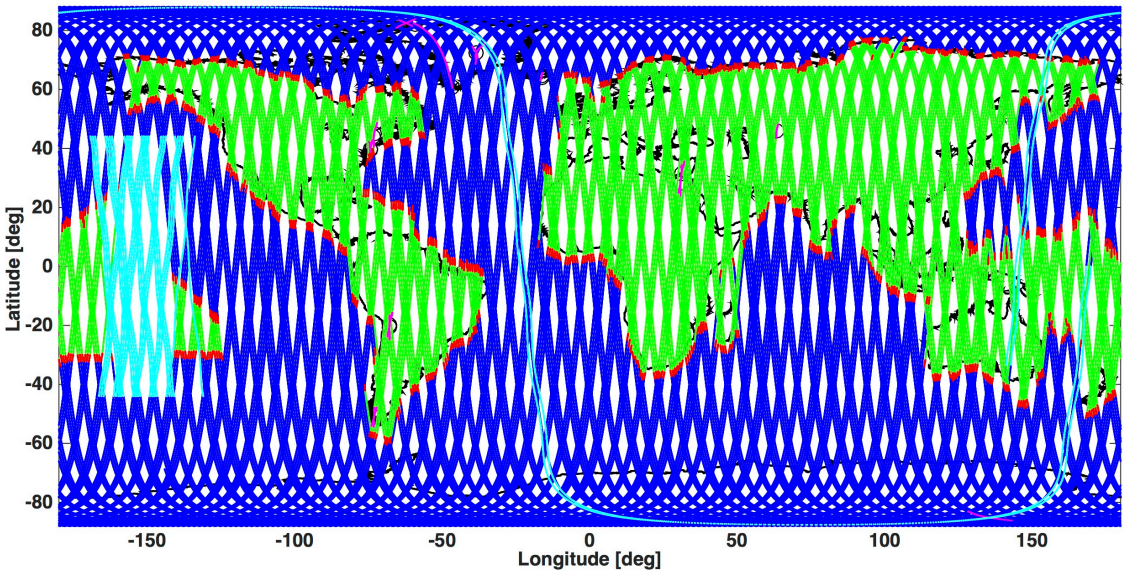

Figure 3-9 Science Activity Map for Spot 7

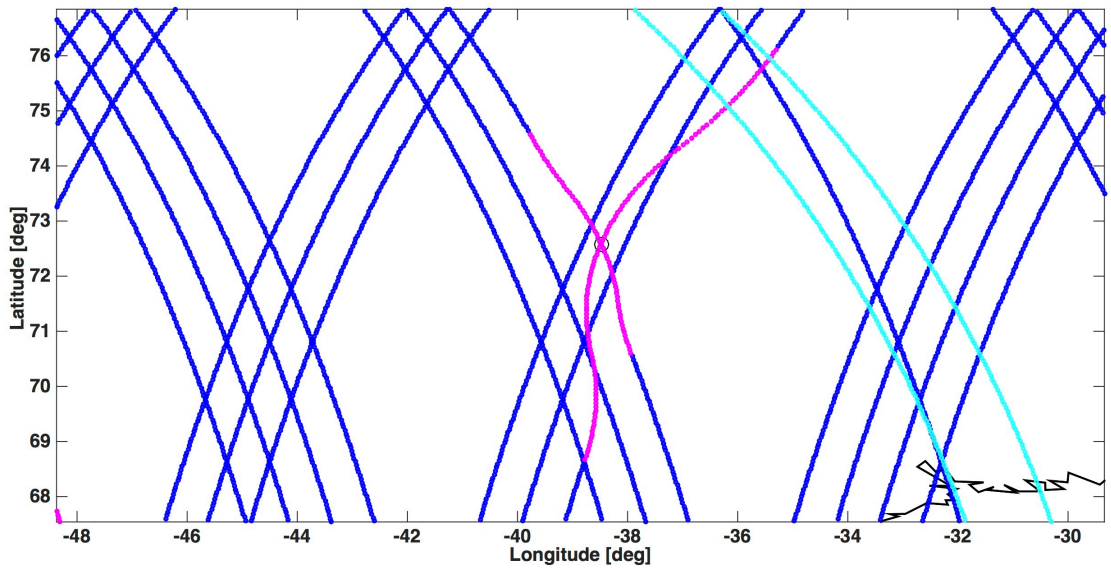

Figure 3-10 Target of Opportunity Laser-Tracks

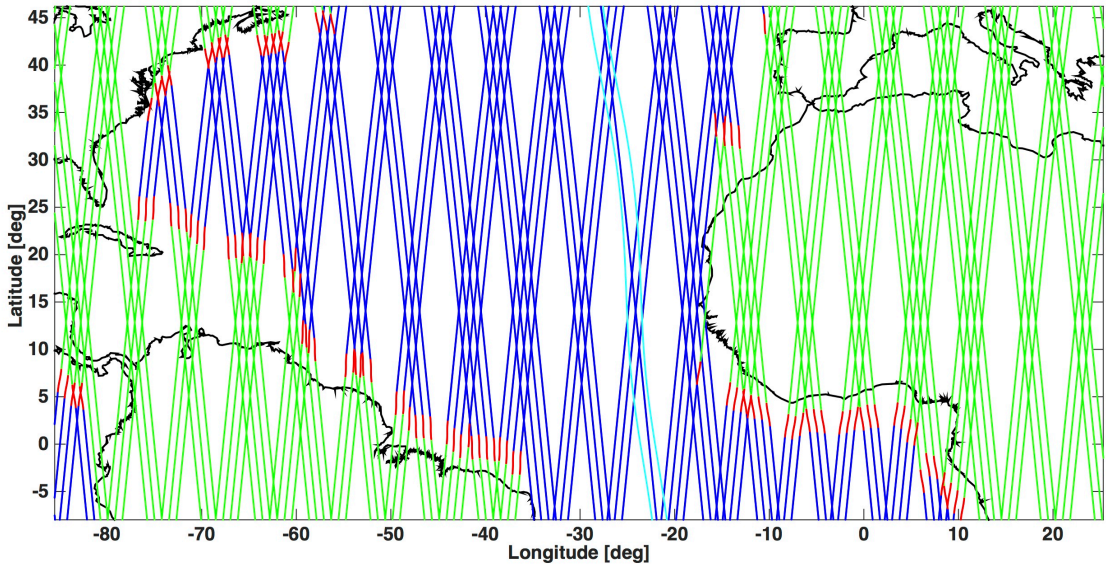

Figure 3-11 Reference Ground-Track Pointing and Vegetation Off-pointing Laser-Tracks

Table 3-8 Simulated Data Products for 14-day Orbit in the Life. To used by the SIPS for testing and validation.

File	Input	Description
ANC03_p_200506052047_v01	$R_{ECI \rightarrow ECF}$	Interpolated from ECI to ECF daily quaternions (Eq. 3.1.9)
ANC04_p_200506052047_v01	$\vec{X}_{s/c}, \vec{V}_{s/c}$	Daily orbit precision ephemeris position and velocity in ECI (Eq. 3.1.6)
*ANC05_p_200506052047_v01	$\hat{L}_{ECI}$	Pointing unit vectors in inertial frame (Eq. 3.1.7)
*LF_2_SF_200506052047_v01.a	$R_{LF \rightarrow SF}$	LF to SF quaternions (Eq. 3.1.7)
*SF_2_J2000_200506052047_v01.a	$R_{SF \rightarrow ECI}$	SF to ECI quaternions (Eq. 3.1.7)
beam7_Roundtrip_Range.txt	o, t_T	Observed round-trip range and transmit time tags for spot 7 which is a fictitious spot at the center of the spot pattern (Eq. 3.1.1)

*Note: Not calibrated

4.0 SUPPORTING ANALYSIS

4.1 Atmospheric refraction path delay dependence on change in geolocation elevation and horizontal position.

Figure 4.1.1 shows the dependence of the atmospheric path delay on photon event bounce point elevation. The dependence is linear at ~2.5 cm in path delay per 100 m in elevation (ATL03r *Atmospheric Refraction Path Delay ATBD*).

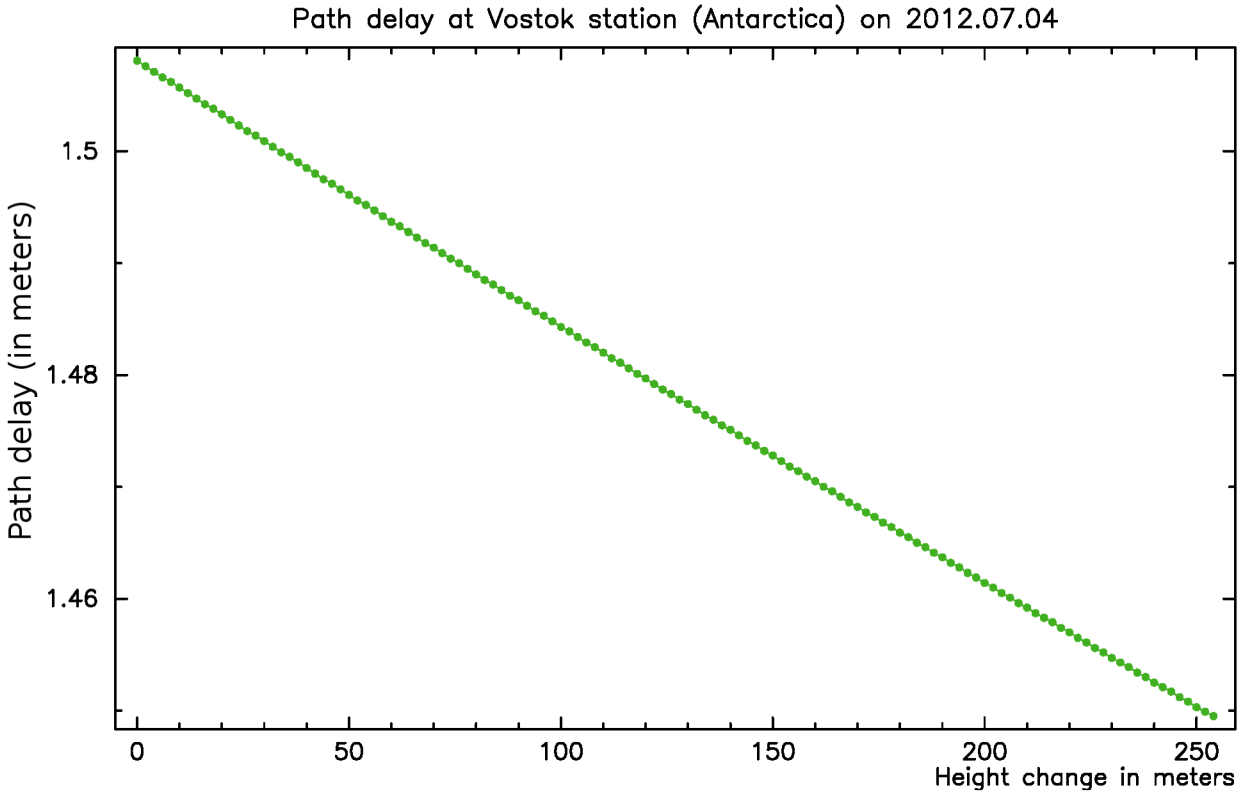

Figure 4-1 Dependence of Path Delay on Elevation at Vostok Station (L. Petrov)

Figure 4.1.2 shows the dependence of the atmospheric path delay on photon event bounce point geolocation horizontal position. At a given altitude the path delay depends on synoptic change of atmospheric pressure. During a typical winter storm the atmospheric pressure fall at 30 mbar at a distance of 1000km, or 0.03 mbar at a distance of 1 km. 0.03 mbar is 0.03/1013 = 3.0E-5 relative change. Since the total path delay at the first approximation is proportional to the surface atmospheric pressure, this variation of the atmospheric pressure changes the total path delay ~2.4 m at a sea level by 3.0E-5, i.e. 2.4*3.0E-5 = 7.1E-5 meter = 0.07 mm over a distance of 1 km. (*L. Petrov, personal communication, and ATL03a Atmospheric Refraction Path Delay ATBD*).

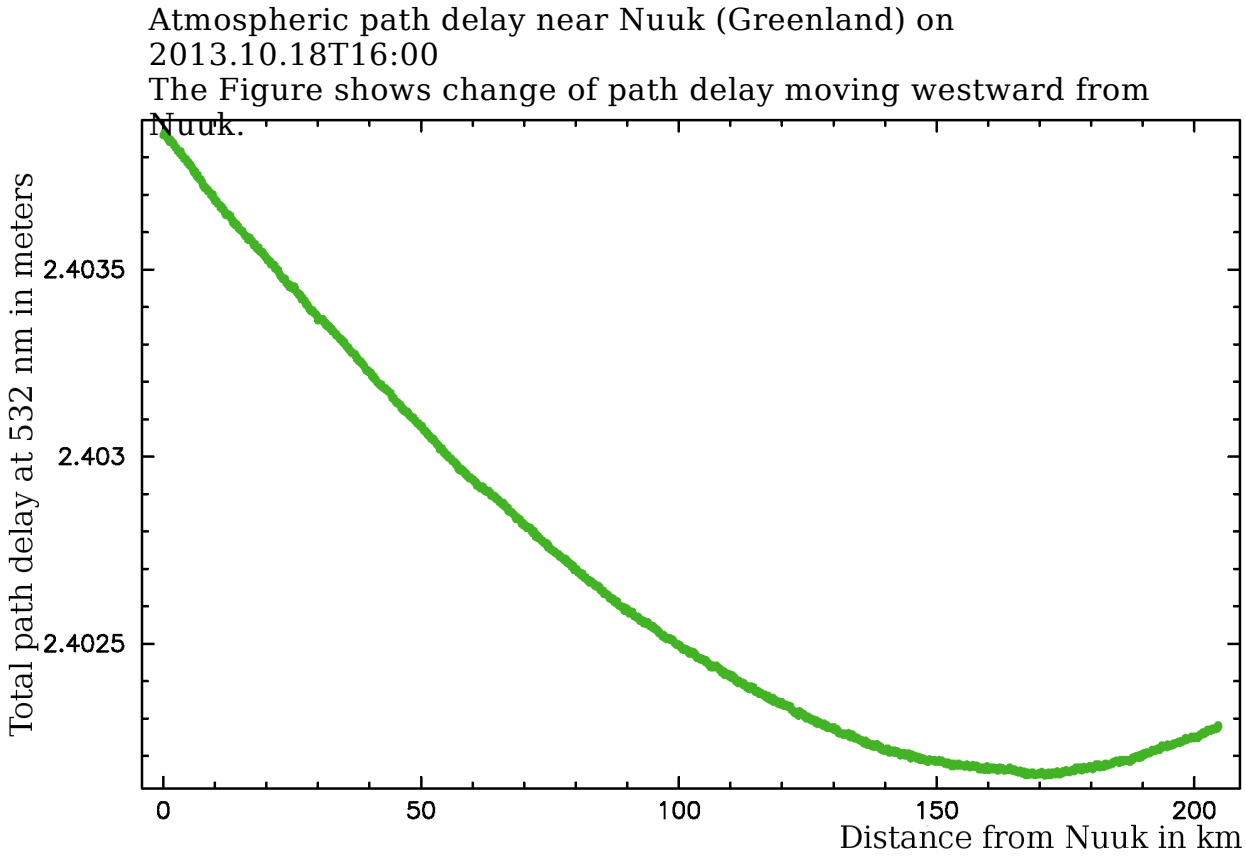

Figure 4-2 Dependence of Path Delay on Geolocation Horizontal Position (L. Petrov)

5.0 REFERENCES

[1] Coppola, V. T., Seago, J. H., Vallado, D. A., "The IAU 2000a and IAU 2006 Precession-nutation Theories and Their Implementation." *American Astronautical Society*. 2009.

[2] Guinot, B., "Report of the Sub-group on Time", in *Reference Systems*, J. A. Hughes, C. A. Smith, and G. H. Kaplan (eds.), U. S. Naval Observatory, Washington, D. C., 3-16, 1991.

[3] Hofmann-Wellenhof, B., H. Lichtenegger, and J. Collins, *GPS: Theory and Practice*, Third Edition, Springer-Verlag, Wien, 1994.

[4] McCarthy, D. D., *IERS Technical Note 21*, July 1996.

[5] Standish, E. M., Newhall X X, Williams, J. G. and Folkner, W. F., 1995, "JPL Planetary and Lunar Ephemerides, DE403/LE403", JPL IOM 314.10-127, 1995.

[6] Petit, G. and B. Luzum, 2010, "IERS Conventions (2010)," IERS Technical Note No. 36, International Earth Rotation and Reference System Service (IERS).

GLOSSARY/ACRONYMS

ASAS	ATLAS Science Algorithm Software
ATBD	Algorithm Theoretical Basis Document
ATLAS	Advance Topographic Laser Altimeter System
ECF	Earth Centered Fixed
ECI	Earth Centered Inertial
GPS	Global Positioning System
ICESat	Ice, Cloud and Land Elevation Satellite
ICRS	International Celestial Reference System
IERS	International Earth Rotation Service
JD	Julian Date
LF	Laser Frame
LRS	Laser Reference System
MIS	Management Information System
MJD	Modified Julian Date
MOC	Mission Operations Center
MRF	Mechanical (Master) Reference Frame
N	Nutation
OBS	Observatory
POD	Precision Orbit Determination
P	Precession
PPD	Precision Pointing Determination
PSO	Project Science Office
R	Earth's spin
SBF	Spacecraft Body Fixed
S/C	Spacecraft
SCoRe	Signature Controlled Request
SDMS	Scheduling and Data Management System
SF	Star Frame
SIPS	Science Investigator-led Processing System
TAI	International Atomic Time
TBD	To Be Determined
TDT	Terrestrial Dynamic Time

TT	Terrestrial Time
UTC	Coordinated Universal Time
W	Polar motion
ZRP	Zero Range Point